Biophys Struct Mech (1982) 8:107–150

Biophysics of Structure and Mechanism

Review

ESR and ENDOR of Primary Reactants in Photosynthesis*

A. J. Hoff

Department of Biophysics, Huygens Laboratory of the State University, P.O. Box 9504, NL-2300 RA Leiden, The Netherlands

Abstract. The primary reactants in photosynthesis are defined as the chemical entities on which charges are generated and stabilized after capture of a photon by the photochemical trap: $PIX \xrightarrow{h\nu} P^*IX \rightarrow P^+I^-X \rightarrow P^+IX^-$, where P stands for the primary electron donor, P^* for its excited singlet state, I for the 'first' (ESR-detectable) electron acceptor and X for the secondary acceptor complex. The ESR and ENDOR experiments which have played a rôle in the identification and characterization of P, I, and X in the bacterial and plant photosystems are comprehensively reviewed. The structural and kinetic information obtained with magnetic resonance techniques are integrated with results obtained with optical spectroscopy to give a unified picture of the pathway of primary photochemistry in photosynthesis.

Key words: Photosynthesis – Primary reactions – ESR – ENDOR – Chlorophyll – Bacteriochlorophyll – Pheophytin – Bacteriopheophytin – Ferredoxin – Iron-sulfur protein

Nomenclature of Primary Reactants

In the interest of uniformity this review introduces a nomenclature of the primary reactants that deviates in some respects from the commonly used labels. The nametags used here and listed below are abbreviations of the molecules that are identified as primary reactants, with the exception of the donors, for which I have retained the commonly accepted designation.

Photosystems: PS 1, photosystem 1 of plants; PS 2, photosystem 2 of plants; pBPS, the photosystem of purple bacteria; gBPS, ditto of green bacteria.

P: Primary donors: P700 (PS 1), P680 (PS 2), P860 (generic label for BChl *a* containing purple bacteria), P960 (generic label for BChl *b* containing purple bacteria), P840 (generic name for green bacteria).

I: 'First' acceptors: Chl *a* (PS 1), Ph *a* (PS 2), BPh *a,b* (pBPS).

X: Secondary acceptors: F_X (PS 1), pQ_1 (PS 2), uQ_1 or mQ_1 (pBPS), B (gBPS).

Tertiary acceptors: $F_{A,B}$ (PS 1), pQ_2 (PS 2), uQ_2 (pBPS), F_1 (gBPS).

* This paper is based on a lecture given at the Joint Meeting of the Belgium, German (FRG), and Netherlands Societies for Biophysics, Aachen 1980

0340-1057/82/0008/0107/$ 08.80

1. Introduction

Electron spin resonance (ESR) and electron-nuclear double resonance (ENDOR) techniques have contributed much to the identification of electron carriers in photosynthesis. Moreover, with the aid of these techniques their interactions and organization in the photosynthetic membrane could be investigated and information obtained about the pathway of primary reactions. In conjunction with other physical techniques, as fast optical spectroscopy, and the recent progress made in the biochemical isolation of reaction center particles, a unified picture is now developing of the primary light reaction in the three photosystems generally thought to exist, viz. photosystem 1 and 2 in plants (PS 1, PS 2) and the single photosystem in photosynthetic bacteria [the Bacterial Photosystem, subdivided in one for purple non-sulphur bacteria (pBPS) and one for green sulphur bacteria (gBPS)]. In this article I will attempt to give a synthesis of the available data with emphasis on the recent contributions of ESR and ENDOR. A comprehensive review of ESR and ENDOR work in photosynthesis up to and including 1979 can be found in [1]; I will assume that the reader has a general knowledge of the plant and bacterial photosynthetic systems, see e.g. [2].

1.1 The Primary Light Reaction

A schematic survey of the photosynthetic electron transport in the plant and bacterial photosystems is displayed in Fig. 1a.

The generic formula for the primary light-induced charge separation reads

$$PIX \overset{h\nu}{\rightarrow} P^*IX \rightarrow P^+I^-X \rightarrow P^+IX^-. \tag{1}$$

Here, P denotes the primary electron donor, I the first electron acceptor, X the secondary acceptor. P is usually labeled with a number indicating the wavelength in nm at which a bleaching is observed in an optical absorption difference spectrum (light−dark): P700 (plant photosystem 1), P680 (plant photosystem 2). In the purple, non-sulphur photosynthetic bacteria that contain solely BChl *a*, the above wavelength is about 860 nm, varying somewhat from species to species. In addition, it is dependent on temperature, shifting some 25 nm to the red at temperatures of 77 K and below. In this article I will use P860 generically as the label of the donor for these bacteria. Purple bacteria containing BChl *b* show a bleaching at much longer wavelength, owing to the structural difference between BChl *a* and *b* (Fig. 1c); I will use P960 as the label for their primary donor. In the green, sulphur metabolizing photosynthetic bacteria, the bleaching occurs at about 840 nm, and the primary donor will be labeled P840.

The secondary acceptor X is a one-electron acceptor, it passes its electron on to a subsequent acceptor that is either a two-electron gate (PS 2, pBPS) or, presumably, another one-electron acceptor (PS 1). From there on the electron is shuttled along the various electron transport chains, for more details see, e.g.,

[2]. The primary donor is readied for another turnover by rapid reduction by an electron donor that is either located in the membrane as part of the electron transport chain (PS 2) or is a mobile water-soluble electron carrier as cytochrome c_2 (pBPS) or the copper protein plastocyanin (PS 1).

1.2 The Balance Between Forward and Back Reactions

At first sight, the extensive list of first, second, third etc. acceptors in the various photoreactions (Table 1a) is bewildering and one might ask oneself why in heaven's name Nature has chosen so many components in the electron transport chain that have become apparent via ESR, optical difference spectroscopy, etc. The answer lies in the requirement that wasteful back reactions must be

Table 1a. g-values of primary reactants[a]

	Donor	'First' acceptor	Secondary acceptor		Tertiary acceptor[b]	
				F_X	F_B	F_A
PS 1	2.0026 (2)	2.0033 (2)	g_x g_y g_z	2.08 1.87 1.76	2.07 1.93 1.88	2.05 1.94 1.86
PS 2	2.0026 (2)	2.0033 (2)		1.82–1.84[c] 2.0044 (3)[d]	–	
pBPS (BChl *a*)	2.0026 (2)	2.0036 (2)		1.8[e] 2.0046 (2)[d]	1.8[e]	
(BChl *b*)	2.0026 (2)	2.0036 (2)		1.8[e]	–	
gBPS	2.0026 (2)	–		2.0040 (5)	(2.05) 1.94 1.88	

[a] Representative values culled from the literature cited in the text
[b] In the doubly reduced state $F_B^- F_A^-$ a third set appears: g = 2.06, 1.92, and 1.89 and the feature at g = 1.86 disappears
[c] Baseline crossing of a $d\chi''/dH$ spectrum
[d] In preparations in which the iron is magnetically uncoupled from the quinone
[e] The $d\chi''/dH$ spectrum shows a baseline crossing at $g \approx 1.82$ and a trough at $g \approx 1.68$ (these values vary somewhat with species)

Table 1b. g-values of electrochemically prepared cation an anion radicals of some chlorophylls and pheophytins

	Cation	Solvent	Reference	Anion	Solvent	Reference
Chl *a*	2.0025 (1)	CH_2Cl_2	[242]	2.0029 (1)	DMF	[173]
Ph *a*	2.0026 (1)	CH_2Cl_2	[243]	2.0030 (1)	DMF	[173]
BChl *a*	2.0025 (1)	CH_2Cl_2	[243]	2.0028 (2)	THF	[244]
BPh *a*	2.0025 (1)	CH_2Cl_2	[243]	2.0030 (2)	CH_2Cl_2	[244]
BChl *b*	2.0025	CH_2Cl_2/CH_3OH 6:1	[157]	2.0033 (2)	THF, DMF	[157]
BPh *b*	–			2.0033 (2)	THF, DMF	[157]

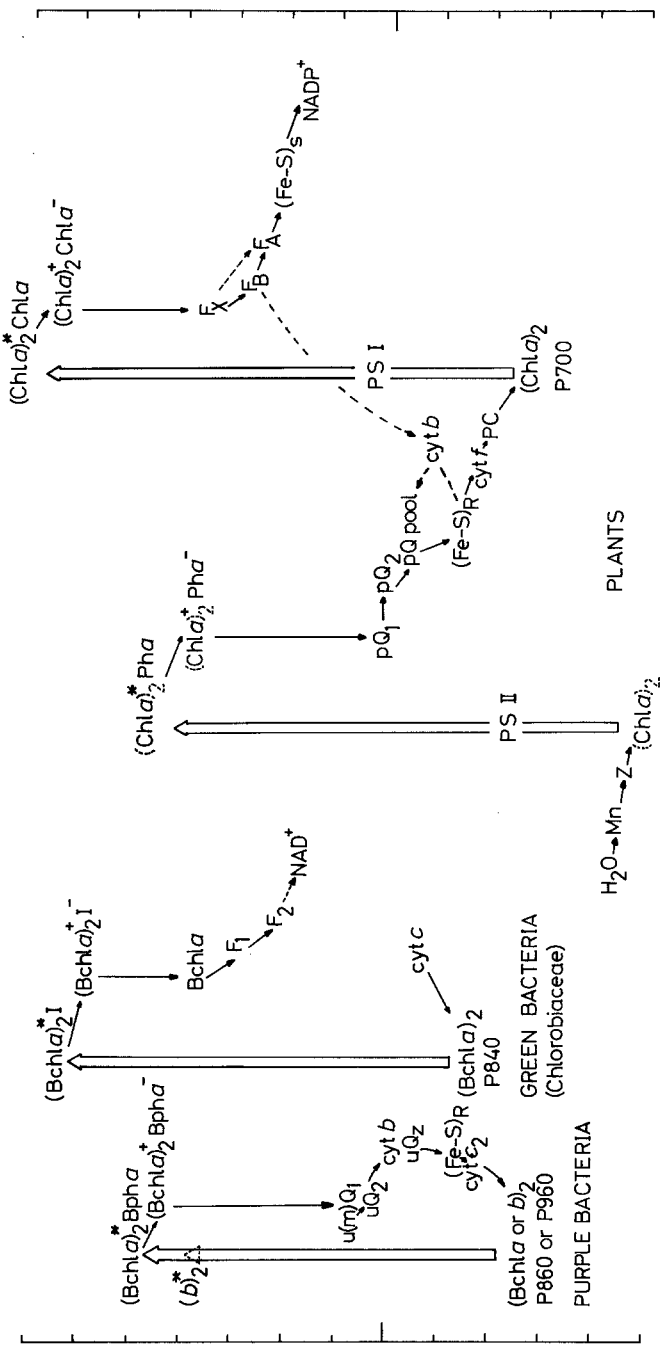

Fig. 1a. Schematic representation of the photosynthetic reactions on a redox scale. Most symbols are explained in the text. Other symbols: PS I, PS II: photosystem 1, 2, $(b)_2^*$: excited state of the primary donor in BChl *b* containing bacterial species, uQ_2: ubiquinone involved in the oxidation of cyt *b*, NAD(P): nicotinamide adenine dinucleotide (phosphate), [Mn]: charge accumulating Mn containing protein involved in the splitting of water, *Z*: secondary donor of PS 2, *pQ* pool: pool of 'unbound' plastoquinones mediating electron transport between PS 2 and PS 1, $(Fe-S)_R$: 'Rieske' iron-sulfur protein, *PC* plastocyanin (a Cu containing protein), $(Fe-S)_S$: soluble ferredoxin. The reduction of $NAD(P)^+$ involves one or more proteins that are not indicated. Cyclic pathways in green bacteria and plants are omitted. An asterisks indicates the photoexcited state of the primary donor. For the purple bacteria and PS 2, and by inference for the other photosystems, the energy level of the geminate radical pair after the initial charge separation is close (ΔE = 50–100 mV) to the photoexcited state; it does not correspond to the redox level of the first acceptor as determined by chemical reduction. All other components have been set at the midpoint redox potential as measured by chemical redox titration. Their potential in the working electron transport chain may be different, e.g., due to photoinduced neighbouring charges

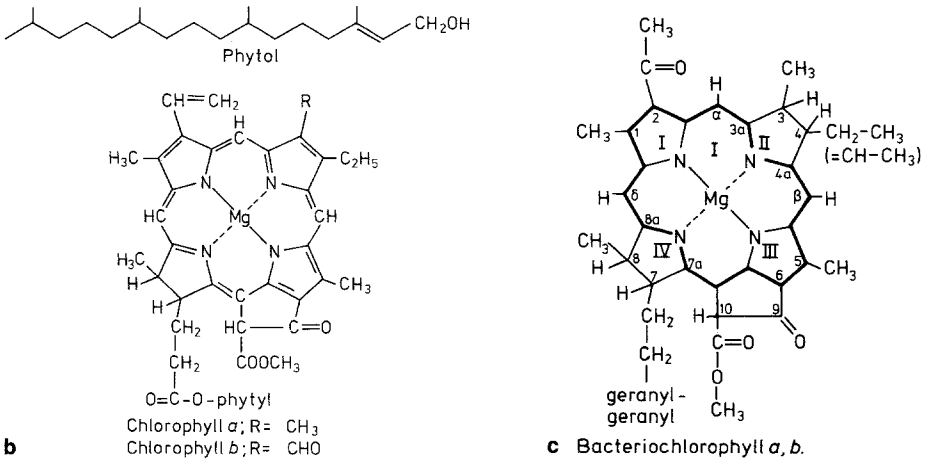

Fig. 1b and c. Chlorophyll *a* and *b* (**b**) and bacteriochlorophyll *a* and *b* (**c**). Molecules without the central Mg atom are called (bacterio)pheophytin. BChl *b* has a = $CH\text{-}CH_3$ group attached to C_4 in ring II instead of an ethyl group

prevented. Obviously, would after the charge separation $PI \xrightarrow{h\nu} P^*I \rightarrow P^+I^-$ the unpaired electrons recombine with appreciable yield to the ground state *PI* in competition with the forward reaction $I^-X \rightarrow IX^-$, then photosynthesis would be an inefficient process. It is precisely this back reaction that makes artificial cells emulating the primary photoreactions very inefficient compared to Nature's way.

The chemical free energy contained in a radical pair is the sum of their midpoint redox potentials

$$E(P^+I^-) = \mid E_m(P/P^+) \mid + \mid E_m(I/I^-) \mid .$$

This energy must be degraded to prevent back reaction to the excited state P^*I from which charge separation proceeds (note that, because of multiple charge separation and recombination processes, 10–20% of back reaction to P^* may be tolerated). On the other hand, energetically down-hill electron transfer is slowed when the energy gap to be bridged is too broad. Apparently, the right balance is struck when between the primary donor and the stable acceptor from which slow biochemical redox reactions may proceed, a number of intermediates are placed at more or less regular intervals on a redox scale. These intermediates are closely coupled to each other, and electron transport is governed by vibrationally coupled electron 'hopping'. Back reactions to the higher lying states are inhibited by the Boltzmann factor, and possibly by conformational changes due to Coulombic interactions. The back reactions to the ground state *PIX* . . . from the initial radical pair P^+I^-X is slow because of the large energy gap; from the pair P^+IX^-, . . . and so on, the increasing distance between the charges impedes the back reaction to *PIX* . . .

By virtue of the fact that the various photoinduced cations and anions (Table 1b) in the plant and bacterial photosystems are paramagnetic, ESR and ENDOR have proved to be eminently useful techniques to aid in the detection and

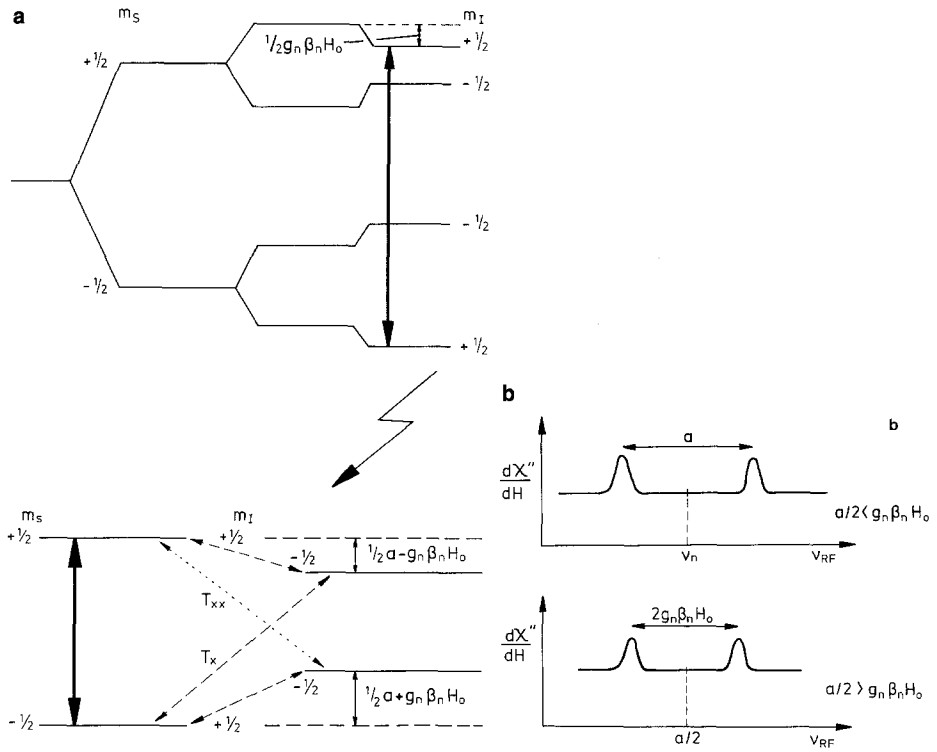

Fig. 2. a Term schemes of a $S = {}^1/_2$, $I = {}^1/_2$ spin system. Heavy arrows indicate ESR transitions ($\Delta m_S = 1$, $\Delta m_I = 0$). In the lower scheme, light arrows indicate ENDOR transitions ($\Delta m_S = 0$, $\Delta m_I = 1$), the heavy arrow represents the half-saturated ESR transition. T_x is an allowed, T_{xx} a spin-forbidden relaxation pathway. **b** Schematic ENDOR spectrum for the spin system of Fig. 1 for $a/2 < g_n\beta_nH_0$ (upper trace) and $a/2 > g_n\beta_nH_0$ (lower trace)

assignment of the primary donors and the various intermediairy and 'final' acceptors. In the following sections I will discuss the identity and structure of *P*, *I*, and *X* (all photosystems) with emphasis on the ESR and ENDOR evidence, the information obtained on the magnetic interactions between their doublet states (P^+, I^-, X^-) and the observations relating to the triplet state of the primary donor, P^T.

2. Basics of ESR and ENDOR

The basic principles of ESR and ENDOR are summarized in Fig. 2. The energy levels of a $S = {}^1/_2$ spin system are split by a magnetic field (the Zeeman effect), the magnitude of the splitting is given by $E = g_e\beta_eH_0$ were g_e is the electronic gyromagnetic ratio (the *g*-factor), β_e the electronic Bohr magneton and H_0 the magnetic field. When an oscillating electromagnetic field, of frequency $\nu = h^{-1}g_e\beta_eH_0$ (h = Planck's constant) is applied, spins may flip up or down and for Boltzmann equilibrium a net absorption of energy from the oscillating field is measured. Usually, the frequency ν is kept constant and the static field H_0 is

scanned, with a sinusoidal modulation of a few Gauss. The absorption of energy at the resonance condition $H_0 = h\nu/g_e\beta_e$ is then recorded as the first derivative of an absorption band; for $g_e = 2$, $H_0 \sim 3{,}300$ G for $\nu \sim 9$ GHz. In Fig. 2a the energy levels are further split by the hyperfine interaction aI_zS_z with a nucleus of spin $I = {}^1/_2$, and by the nuclear Zeeman splitting $g_n\beta_nH_0$ (g_n, β_n the nuclear g-factor and Bohr magneton, respectively). Because of the selection rules $\Delta m_s = 1$, $\Delta m_I = 0$, this results in two ESR lines of equal amplitude. For molecules with many nuclei the ESR lines resulting from the hf interactions overlap. For k sets of n_k equivalent nuclei with nuclear spin I_k there are as many as $\Pi_k(2\, n_kI_k + 1)$ of them; their envelope approaching a Gaussian shape for large n.

The information of the hyperfine interactions observed under the Gaussian ESR lineshape can be extracted by electron-nuclear double resonance (ENDOR), the principle of which is explained in Fig. 2b. If one of the ESR transition (say the one between the $m_I = +{}^1/_2$ levels) is half-saturated, irradiation of a nuclear spin transition opens up a new relaxation channel, and an enhancement of the ESR line will result (Fig. 2b). The ENDOR resonance condition is $h\nu_{\mathrm{ENDOR}} = |\, {}^1/_2\, a - g_n\beta_nH_0 \,|$, the two possibilities $a/2 < g_n\beta_nH_0$ and $a/2 > g_n\beta_nH_0$ are displayed and it is seen that for the former case the ENDOR resonance lines are separated by the hyperfine coupling a. The value of a is usually given in MHz, as the frequency of the nuclear magnetic resonance lies in the radio frequency range ($g_n\beta_n$ being about a thousand times smaller than $g_e\beta_e$). The great advantage of ENDOR lies in its simplification of the resonance spectra, as for k sets of n_k equivalent nuclei there are only $2\,k$ ENDOR lines, which are usually very narrow (of the order of 100 kHz).

3. The Primary Donor

3.1 pBPS and PS 1: P860 and P700

The long wavelength at which a bleaching is induced by actinic light or oxydizing chemical agents [3–6] indicated, that P860 is a photooxydizable bacteriochloropyllous species. A photoinduced ESR signal at $g = 2.0$ in photosynthetic bacteria was first observed by Commoner et al. [7] and by Sogo et al. [8]. It was later established that it is formed in a 1 : 1 stoichiometry with the light-induced bleaching [9, 10] (which has a quantum yield close to 1.0 [11, 12]), that the risetime is less than 5 ns [13], that it is reversibly photo-induced at low temperature, down to 1.5 K [14], that it has the same action spectrum [17, 18] as the optical bleaching when observed simultaneously in an optical transmission ESR cavity and the same decay kinetics [10, 15, 16, 79], and that, it has a redox midpoint potential similar to that of the optical bleaching (+450–+500 mV [19, 20]). These observations are conclusive in assigning the photo-induced ESR signal to the primary donor of the pBPS. Its spectral characteristics are (Fig. 3): i. the line shape (derivative mode) is purely Gaussian of peak-to-peak width $\Delta H_{p\text{-}p} = 9.4 \pm 0.2$ G at room temperature [20, 21] (the linewidth increases by 0.3 G between 80 and 1.5 K [22]), ii. the g-value is 2.0026 ± 0.0001 [20, 21], iii. it saturates as an inhomogeneously broadened line [23].

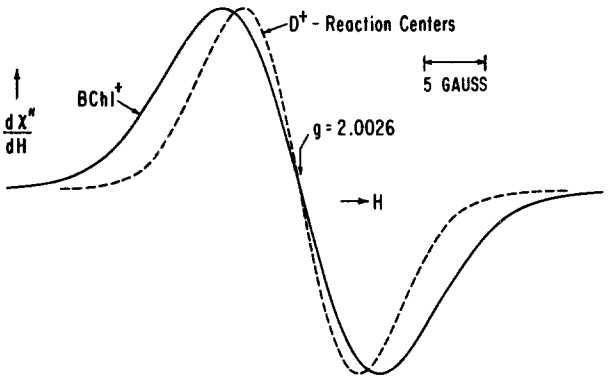

Fig. 3. ESR spectra of $P860^+$ (D^+, dashed line) and BChl a^+ (drawn line) at 77 K [22]

The in vivo ESR signal was compared with that of BChl *a* oxidized in vitro [21, 24]. The BChl a^+ signal showed similar characteristics, except that the linewidth was $\Delta H_{p-p} = 13.0 \pm 0.2$ G, i.e., a factor 1.4 wider than the in vivo ESR signal. This factor 1.4 is found for practically all BChl *a* containing purple bacteria, and also for Chl a^+ compared to $P700^+$ [24]. A careful study was made of factors contributing to the linewidth of $P860^+$ and BChl a^+ (as hyperfine (hf) coupling, *g*-anisotropy), using ESR spectrometry at two frequencies (9 and 35 GHz) and fully protonated and perdeuterated material [21, 24]. It was found that the linewidth component due to the hyperfine coupling with protons (ΔH_p) was dominant over other broadening factors in the protonated samples, with ΔH_p (BChl a^+) $\approx 1.4\,\Delta H_p$ ($P860^+$) (*R. rubrum* [21]). As ΔH_p is proportional to the *square root* of the proton hf coupling (for Gaussian lines, i.e., large *n*, the relation is $\Delta H_p^2 = {}^4/_3\,\Sigma_i n_i I_i (I_i + 1) a_i^2$, with *n* the number of *i* equivalent nuclei with spin I_i and hyperfine coupling constant a_i [25]) the factor 1.4 led Norris et al. [24] to the hypothesis that P860 and P700 are BChl *a* and Chl *a dimers,* respectively, the two pigments sharing the unpaired electron on a timescale at least comparable to the largest hyperfine splittings (about 16 MHz); note that 1 Gauss corresponds to 2.8 MHz).

The dimer hypothesis means that for a symmetric dimer (or 'special pair' in the terminology of Norris et al. [24]) all hf couplings should be halved with respect to those of the chlorophyll cation in vitro. This was demonstrated to be (approximately) true with low temperature ENDOR. As mentioned in Sect. 1, ENDOR is far superior to ESR for the resolution of hyperfine couplings. Simultaneously, and independently, Feher et al. [22, 26], and Norris et al. [27–29] measured the ENDOR spectrum at 77 K of chromatophores [22, 26] and whole cells [27–29] of photosynthetic bacteria, subchloroplast particles enriched in PS 1 [26] and algae [27–29]. Some of the resulting spectra are reproduced in Fig. 4. It is seen that indeed the observable hf splittings of the in vivo preparations are approximately one-half of the corresponding splittings of the in vitro samples.

The assignment of the observed proton ENDOR lines of the BChl a^+ molecule took some effort. We can distinguish 4 classes of protons (Fig. 1c): a) the CH_3 groups on rings I and III, b) the four β-protons (one carbon atom

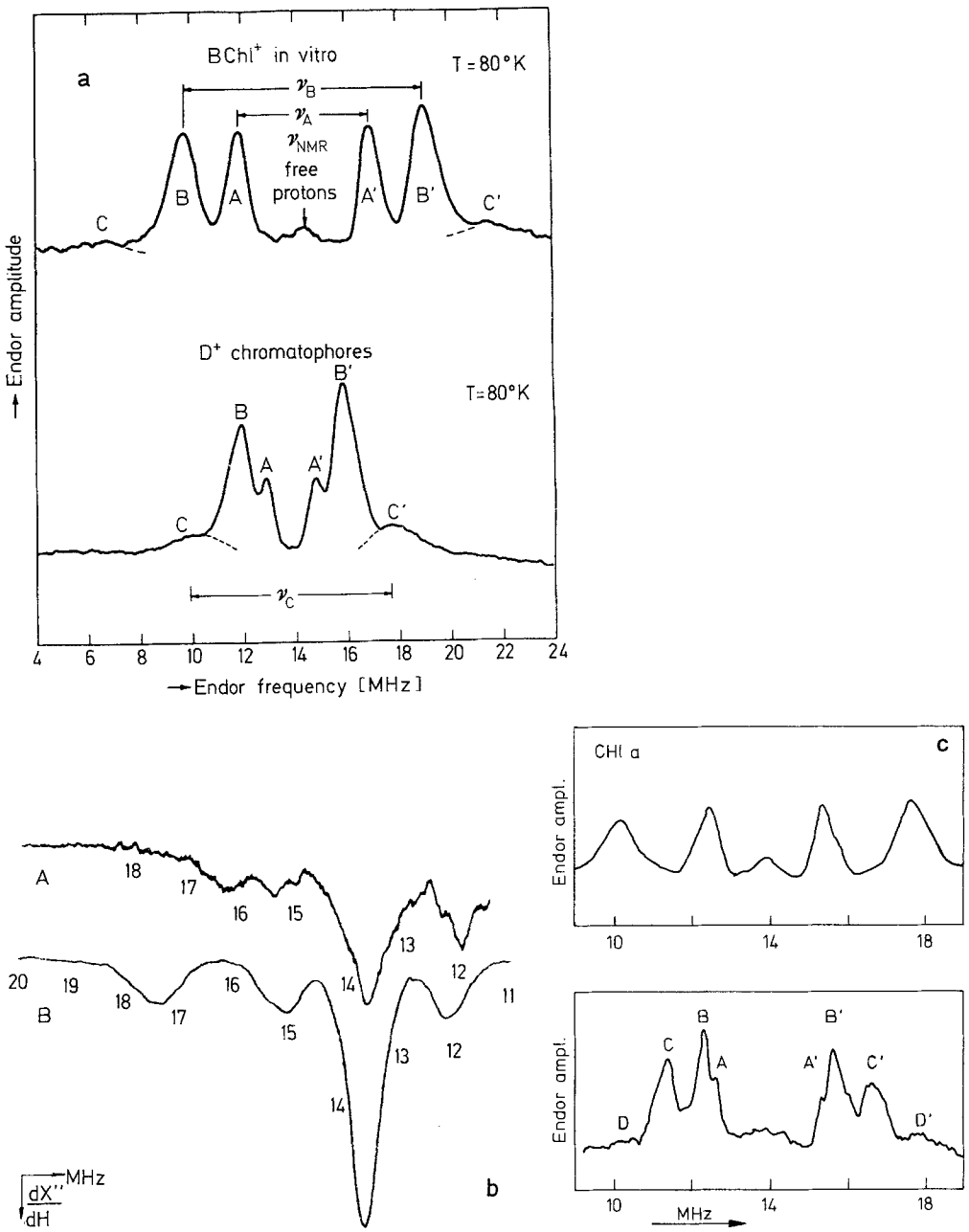

Fig. 4. **a** Comparison of proton ENDOR spectra from BChl a^+ in vitro (top) and chromatophores of *Rps. sphaeroides* R-26 (bottom). The hyperfine splittings ν_A and ν_B for BChl a^+ in vitro and $P860^+$ are 5.0 ± 0.1, 9.2 ± 0.2, and 2.0 ± 0.1, 4.2 ± 0.2 MHz, respectively. The hyperfine splittings *CC'* are approximately 16 and 8 MHz for BChl a^+ and $P860^+$, respectively [22]. **b** Comparison of in vitro and in vivo chlorophyll proton ENDOR at 97 K. A. *C. vulgaris* algae oxidized by $K_3Fe(CN)_6$. B. Chl *a* in $CH_3OH : CH_2Cl_2$ 1 : 3 (v/v) oxidized with I_2 or $FeCl_3$. The strong lines at the free proton frequency (13.7 MHz) are due to matrix ENDOR [29]. **c** Comparison of Chl *a* and $P700^+$ proton ENDOR at 77 K. Top: Chl *a* in C_2H_5OH oxidized with I_2. The hf splittings are 7.5 and 2.9 MHz, respectively. Bottom: light-induced Signal *I* ($P700^+$) in PS 1 subchloroplast particles. The hf splittings are: *DD'*: 7.5, *CC'*: 5.2, *BB'*: 3.4, and *AA'*: 2.7 MHz [1]

away from the conjugated system) in rings II and IV and the β-proton at C10, c) the α-protons on the three methine positions, d) γ-protons, two carbons away from the conjugated rings (various side groups).

Although the protons of the CH_3 groups are β-protons, they are distinct from the other β's because the CH_3 groups rotate rapidly around the 3-fold axis, even at temperatures well below 80 K. In contrast to the ring II and IV β-protons, this renders their (isotropic) hfs insensitive to immobilization by freezing or encapsulation in a protein matrix. They will therefore give rise to sharp low temperature ENDOR lines. The α-protons have strongly anisotropic hfs and are difficult to observe at low temperatures. The γ-protons have very low hfs, their ENDOR lines will be grouped close to the proton free precession frequency, and because their hfs is dependent on geometry, they will be difficult to detect in the frozen state. The ring β-protons see large spin densities on the adjacent carbon atom, but their ENDOR lines are broadened because of the differences in their positions with respect to the chlorophyll plane[1].

The above guidelines serve to provisionally attribute the strong ENDOR lines of Fig. 4a to the two methyl groups and the slight shoulders (C, C') on the outer flanks of lines B, B' to the ring II and IV β-protons. This assignment was checked by selective partial deuteration of the methyl groups, and by partial deuteration of these groups plus deuteration of the α- and β-positions. For the latter preparation the ENDOR lines AA' and BB' persisted, demonstrating that they are due to the CH_3 groups on ring I and III, whereas the shoulders CC' had disappeared. The strong ENDOR lines with largest hfs (lines AA') were assigned to the CH_3 groups on ring I by comparing amplitudes of the strong ENDOR lines of oxidized BChl *a*, Chl *a*, Chl *b*, and Chl *c*, which differ in the number of CH_3 groups (Fig. 1), and assuming that CH_3 groups on rings I, II, and IV were equivalent[2] (ring III is adjacent to the symmetry-breaking ring V). This assignment was corroborated by Norris et al. [28, 30] who compared the spectrum of methylpyrochlorophyllide a^+, in which the ring III methyl group was replaced by ^2H, with that of Chl a^+.

That the methyl groups do rotate at 80 K was demonstrated by a study of the temperature dependence of the linewidth of BChl a^+ between 1.5 and 80 K, and by ENDOR spectra of BChl a^+ in this temperature range [22]. If rotation of a methyl group is stopped one expects its contribution to the linewidth to increase by a factor of $(3/2)^{1/2}$ [22]. Indeed it was found that the linewidth of protonated, partially and fully deuterated BChl a^+ increased (by 0.5, 2.0, and 0.5 G respectively) going from 80 to 1.5 K (in the partially deuterated sample the β-positions were fully deuterated and the methyl groups partially deuterated, rendering this sample most sensitive to the effect of hindered $CH_{1.5}D_{1.5}$ rotation). Concomitantly, the ENDOR spectra showed a broadening and congealing of the CH_3 lines.

1 The hfs of β-protons is given by: $a_\beta = (B_0 + B_1 \cos^2\theta)\varrho^\pi$, where B_0 and B_1 are constants ($B_1/B_{10} \approx 10$), θ is the dihedral angle between the C_α π orbital and the C_α–C_β–H plane, and ϱ^π is the spin density on the C_α atom. For rotating CH_3 groups $\cos^2\theta = {}^1/_2$ and $a_\beta \sim {}^1/_2\, B_1\, \varrho^\pi \sim 150\, \varrho^\pi$ MHz

2 A shoulder on the inner lines of Chl *a* and Chl *b* can be assigned to the methylene group of ring II ([115, 117] and Fig. 3.2b of [1])

The assignment of BChl a^+ ENDOR lines was further corroborated by liquid state ENDOR studies at high radio frequency power [31, 32] (Fig. 5c). In the liquid state the BChl *a* molecules are rapidly tumbling, thus averaging out the α-proton hfs anisotropy and deviations of the ring β-proton positions from their equilibrium position. Indeed, the β-protons were now clearly observed as sharp lines, and the α-protons and possibly some γ-protons could be discerned [31, 32]. Triple ENDOR studies permitted the determination of the sign of the hfs, strengthening the assignment of the various lines to α- or β-protons [32]. In addition, ^{14}N ENDOR signals could be observed [32] (Fig. 5d), the corresponding nitrogen hfs agreeing well with previous estimates [21, 31].

For the pBPS, we have so far discussed only experiments on BChl *a* containing reaction centers. The oxidized P960 of the BChl *b* containing *Rps. viridis* and *Thiocapsa pfennigii* exhibit a Gaussian ESR line at $g = 2.0025$; but, in contrast to BChl *a* containing species, their linewidth $\Delta H_{p\text{-}p}$ is close to the monomeric value, viz. 14.0 G for the monomer [156], 11.8 ± 0.2 G (*Rps. viridis* [33, 34]) and ~ 13.0 G (*T. pfennigii* [158]) for $P960^+$, respectively. Thus, the in vivo ΔH deviates considerably from that expected for a dimer ($1/\sqrt{2} \times 14 = 9.9$ G). Yet it is not likely that P960 is a monomer, because upon oxidation a band at 1310 nm appears which is not present for BChl b^+ and which most probably corresponds to the 1245 nm band for $P860^+$ [156]. The deviating width of the ESR line of $P960^+$ might be explained by assuming that either electron hopping between members of the pair is slow on an ESR time scale, yielding hfs values intermediate between those of a monomer and those of a dimer, or that in the dimer structure some β-protons are twisted from the position they have in a monomer. Since these protons contribute heavily to the linewidth a slight shift is sufficient to increase considerably the calculated width for $P960^+$.

ENDOR experiments on BChl b^+ were performed by Fajer et al. [156, 157] who found proton hfs of 0.4, 1.7, 3.2, and ~ 4.6 G at −140° C, which compare to corresponding values of 1.7, 3.4, and ~ 5 G for BChl a^+. For *Rps. viridis* $P960^+$ the ENDOR hfs are 1.5, 1.9, 3.3, and 4.0 G [33, 34, 157]. To CH_3 groups were assigned the 1.7 and 3.2 G (BChl b^+) and the 1.0, 1.5 and 1.9 G ($P960^+$) splittings; the other hfs were attributed to β-protons. Simulations of the ESR lines of BChl b^+ and $P960^+$ based on these assignments yielded good fits. This and the narrowness of the ENDOR lines (slow hopping would have broadened them) suggests that either the β-protons are twisted, or that the dimer is asymmetric with unequal electron sharing between the members of the pair. Support for a P960 dimer also comes from the zero field splitting parameters of the triplet state in *Rps. viridis,* which show a reduction of about 25% compared to the triplet state of the BChl *b* monomer (see Sect. 6).

The geometric structure of the dimer is still a matter of speculation (see for reviews, e.g., [35] and [36]). As chlorophylls in vitro are only photooxidizable in the absence of electron acceptors when they are ligated to water (and then forming oligomers) and because such hydrated species show a pronounced shift of their long wavelength absorption band, the hypothesis was advanced that the dimer was 'glued' together by one [37] or two [38] H_2O bridges, one of them linking the central Mg (which is penta-coordinated) to a keto- [37] or ester-oxygen [38]. Recent evidence, however, points to the possibility that the

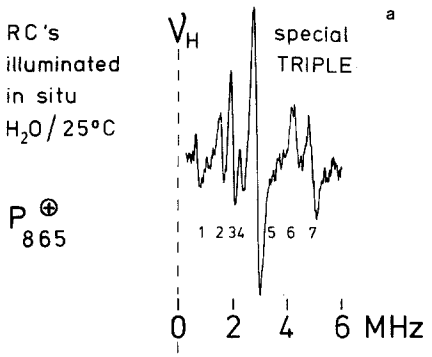

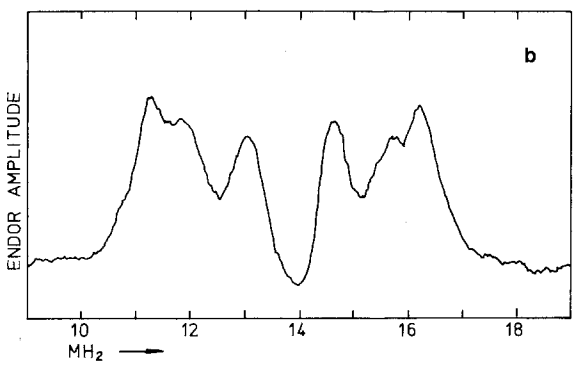

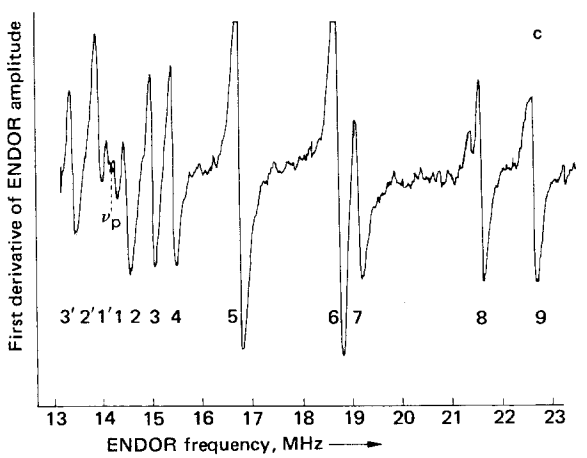

Fig. 5. **a** High power proton ENDOR spectrum of $P860^+$ in reaction centers of *Rps. sphaeroides* R-26 at 25° C. With the special TRIPLE resonance technique both ENDOR lines at $\nu_H \pm {}^1/_2$ a are simultaneously irradiated, giving enhanced ENDOR amplitude and resolution (from [43]). **b** Low power proton ENDOR spectrum of $P860^+$ in reaction centers of *Rps. sphaeroides* R-26 at 80 K (Hoff, Feher, and Isaacson, unpublished results). **c** High power proton ENDOR spectrum of BChl a^+ in liquid CH_2Cl_2/CH_3OH (6 : 1) at 212 K. Lines 5 and 6 correspond to lines A' and B', and lines 7, 8, and 9 to line C' of Fig. 4a. ν_p is the free proton frequency [32]

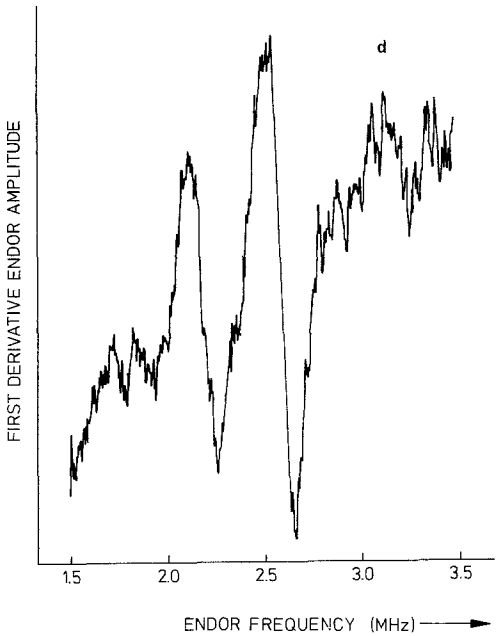

Fig. 5d. High power nitrogen ENDOR spectrum of BChl a^+ in liquid CH_2Cl_2/CH_3OH (6 : 1) at 256 K. The two lines correspond to the high frequency transitions corresponding to two hf splittings of 2.36 and 3.18 MHz, respectively (ν_N = 1.01 MHz at the magnetic field used). For instrumental reasons, the low frequency transitions could not be observed [32]

ligands of the Mg and the keto- and/or ester-oxygen are protein moieties [39–41].

As for the topology, like distance and angle between the planes of the macrocycles, no consensus has been reached. I have discussed the available evidence elsewhere [36, 42] and the reader is referred to these articles for more details.

Very recently, the body of data on the hyperfine couplings of reaction centers has been greatly augmented by high power, high resolution, liquid solution ENDOR [43] of reaction centers of *Rps. sphaeroides* R-26. The spectrum is displayed in Fig. 5a; for comparison an earlier low temperature spectrum of such reaction centers and the liquid solution spectrum of BChl a^+ in vitro [32] are reproduced in Fig. 5b,c. Although the low temperature spectrum is somewhat different from the low temperature spectrum of chromatophores (Fig. 4a), pointing to a slight alteration in the structure due to the isolation procedure, it is clear that the high temperature spectrum deviates considerably from the low temperature spectra of both reaction centers and chromatophores, and that most of the hf couplings are not equal to half of those of BChl a^+ in vitro. As yet, the high temperature spectrum has not been interpreted, but one may hope that it will yield information on questions as the symmetry of the dimer

(if the symmetry is not C2, one may expect unequal sharing of the unpaired spin density over the set of corresponding carbon nuclei).

By and large the spectral characteristics of the ESR signal of $P700^+$ (often called signal I) are very similar to that of P860. It is an inhomogeneously broadened Gaussian, with g-values 2.0025 ± 0.0001, and width $\Delta H_{p\text{-}p} = 7.2 \pm 0.1$ G [44], i.e., 1.4 times smaller than the ESR signal of Chl a^+. Its redox potential is somewhat controversial, ranging from +360 to +520 mV [45–50]; a recently determined value is about +490 mV [51]. The rise kinetics of signal I is instrument-limited, currently 5 ns by spin-echo spectrometry [52]. Its decay kinetics are dependent on temperature and redox conditions [44, 53–60], its light-induction becomes gradually irreversible between 100 K and 20 K in samples frozen at moderate redox potential [56, 58, 61–67]. In general terms its kinetics correlate very well with those optically measured monitoring the bleaching at 700 nm.

As discussed above, the difference in width by a factor of 1.4 between $P700^+$ and Chl a^+ points to P700 being a Chl *a* dimer. This has been checked by low temperature ENDOR [22, 27–29]. The major hf couplings, which are due to rotating methyl groups, are indeed halved in $P700^+$ compared to Chl a^+ (Fig. 4b), but some caution should be exerted, as depending on the conditions, the in vivo sample shows additional lines (Fig. 4c). This may be related to the observation of additional lines in the high temperature ENDOR spectrum of $P860^+$ reproduced in Fig. 5a.

All in all the ESR and ENDOR data on $P860^+$ and $P700^+$ show many similarities suggesting that these two primary donors are homologous with respect to their structure. However, a divergent view has recently been propounded by Wasielewski et al. [68] who, noting that the difference in redox potential of the couples P860/$P860^+$ and BChl *a*/BChl a^+ (0.12–0.23 V [6, 69, 70] is much less than that of the couples P700/$P700^+$ and Chl *a*/Chl a^+ (about 0.4 V [51, 71]), suggested that the monomeric enol form of Chl *a*, in which the ring V keto group is enolized, is a more likely candidate. This compound, trapped as a silyl enol ether, is about +0.35 V easier to oxidize than Chl *a*. The ESR linewidth of its cation was reported to be $\Delta H_{p\text{-}p} = 6.1$ G (a consequence of ring V now being part of the conjugated system) and its ENDOR spectrum is consistent with that of P700 (Fig. 4b). This is an interesting proposal, but it needs backing up by other experiments, e.g., difference resonance Raman studies on PS 1 particles with low Chl *a* content.

3.2 gBPS: P840

In the green bacterial photosystem the difficulty of obtaining purified reaction center preparations has impeded the study of electron transport by means of optical and ESR spectroscopy. Only recently, such particles have been prepared and characterized for the green bacterium *Prosthecochloris aestuarii* [72–76]. The photooxidized primary donor, $P840^+$, gives rise to an ESR signal of Gaussian shape, at $g = 2.0025 \pm 0.0002$ and with $\Delta H_{p\text{-}p} = 9.0 \pm 0.2$ G (at 5 K [75]). This signal is quite analogous to that found for the pBPS, and we may

safely conclude that also P840 is a dimer of BChl *a* molecules [72, 75]. Its midpoint potential is +250 mV [72], i.e., about 200 mV less positive than that of P860 of the pBPS.

Photooxidation of P840 at low temperature in the highly purified reaction centers at ambient redox potential is only partly reversible [75], it is completely irreversible in membrane fragments [77, 78]. When photooxidation is carried out at −520 mV, it becomes completely reversible [75], indicating that irreversibility is caused by electron transfer to a distal acceptor. The decay half-time of the reversible signal is 13 ms, i.e., about twice as fast as in *R. rubrum;* it is presumably due to the back reaction of $P840^+$ and a reduced proximal acceptor [74, 75]. In particles at ambient redox potential in which $P840^+$ is partly reversibly photooxidized, the back reaction generates the triplet state $P840^T$ [74, 75] indicating that in this case electron transfer to the proximal acceptor is blocked because of structural alterations in the reaction center caused by the isolation procedure (for $P840^T$ see Sect. 6).

3.3 PS 2: P680

In intact systems, the photooxidized primary donor of PS 2, $P680^+$, is at all temperatures rapidly reduced. At low temperatures (at 77 K or below) the donor is a cyt b_{559} molecule, at high temperatures it is the 'normal' donor which is part of the linear electron transport chain from water to P680. As a consequence, the ESR signal of $P680^+$ can only be observed at low temperatures and high redox potential, when cyt b_{559} is oxidized [80−83].

Flash illumination then excites an ESR transient of $P680^+$, the signal disappearing because of the back reaction $P^+X^- \rightarrow PX$. The spectrum of this transient consists of a Gaussian line of *g*-value 2.002 and width $\Delta H_{p\text{-}p} = 7-9$ G [81−84]. Because this signal overlaps signal *I* of $P700^+$, the latter signal was irreversibly generated (by low-temperature preillumination or chemical oxidation) and subtracted.

The advent of subchloroplast particles enriched in PS 2 made it possible to accumulate $P680^+$ without interference with $P700^+$. Again, an ESR line very similar to that of $P700^+$ in shape, *g*-value and width was observed [85, 86]. The above data suggest that P680 is a Chl *a* dimer. However, the midpoint redox potential (> 0.9 V) of P680 is much higher than that of P700 (~ +0.4 V) and is much closer to the halfwave oxidation potential of Chl *a* (~ +0.8 V, depending on the solvent [71]). Therefore, it has been proposed that P680 is a Chl *a monomer,* and that the reduction in linewidth is caused by the β-protons of P680 having a larger dihedral angle than those of Chl *a* in vitro [71]. In fact, rather large variations in the linewidth of electrochemically produced Chl $a^+ \cdot ClO_4^-$ ($\Delta H_{p\text{-}p} = 7.8-9.2$ G) were observed for different solvents and attributed to changes in the hf splitting of the β-protons of ring IV [71]. This reduction of the β-hf splitting may be caused by ligand-induced mixing of the ground state $^2A_2$ with some $^2B_2$ excited state character [71]. Model calculations show that the vide infra energy of the $^2B_2$ state, which carries smaller spin densities at the α-carbons of the saturated ring than the $^2A_2$ ground state, lies only just above the $^2A_2$ state.

Moreover, the optical absorption difference spectrum $P680^+ - P680$ and Chl $a^+ -$ Chl a (monomer) are very similar if a shift of about +15 nm is applied to the Chl a spectrum [71]. Apparently, more experimentation is needed to sort out the 'multiplicity' of P680.

4. The Secondary Acceptors, X

As chronologically, the acceptors X were discovered and described before the 'first' acceptors I; they were labeled 'primary' acceptors. With present day knowledge, this nomenclature doesn't make much sense, and I will subsequently refer to them as secondary acceptors. They are well characterized, and I will discuss them before the somewhat less characterized 'first' acceptors, I.

4.1 The Secondary Acceptor of the Bacterial Photosystems

4.1.1 Purple Bacteria, pBPS. The secondary acceptor of the pBPS has various labels, X, UQ, Q etc. It is convenient to use Q, with prefix u for the benzoquinone, ubiquinone, which usually is the acceptor, and m for menaquinone, a naphthoquinone that in some bacterial species (*C. vinosum* and *Rps. viridis*) replaces ubiquinone. By optical absorption difference spectroscopy it was established that the (then called primary) acceptor in the pBPS (exemplified by *Rps. sphaeroides* and *R. rubrum*) is a (ubi) quinone [87, 88]. In contrast, ESR studies showed a very broad line with g-value at ~ 1.8 [89, 90], quite unlike the spectrum of semiquinone radicals (Fig. 6a). The discrepancy was solved by Loach and Hall [91] and Feher et al. [92], who established that upon treatment of reaction center particles with alkali, urea and the detergent sodium dodecyl sulphate (SDS) [91] or with a mixture of two detergents (SDS and lauryl dimethylamineoxide, LDAO) [92], illumination in the presence of the reductant ferrocytochrome c (which reduces $P860^+$) caused an ESR line to appear, with width $\Delta H_{p\text{-}p} = 8.1 \pm 0.5$ G at g-value 2.0046 ± 0.0002 (data from [92], those of [91] are slightly different). The shape of the signal was slightly asymmetric, it was photoproduced in a ratio 1 : 1 to that of $P860^+$ and its Q-band (35 GHz) ESR spectrum showed the characteristic shape of a semiquinone radical [92] (Fig. 6b). As the primary photoreaction proceeds quite normally in the above particles, this means that quinone is the secondary acceptor and that the ESR signal is broadened and shifted because of magnetic interactions with another paramagnetic species. In view of the fact that normally there is 1 Fe per reaction center, but in the treated particles the Fe content was below 0.4 Fe per reaction center, the broadening agent presumably is iron. Replacing Fe by Mn induced little change in the spectrum of normal reaction centers [93], and Mössbauer experiments showed that the Fe remains in a (unusual) high spin $S = 2$, Fe^{2+} state during photoreduction of the secondary acceptor [94]. Put together, the evidence strongly suggests that Q alone is receiving the electron. Apparently the

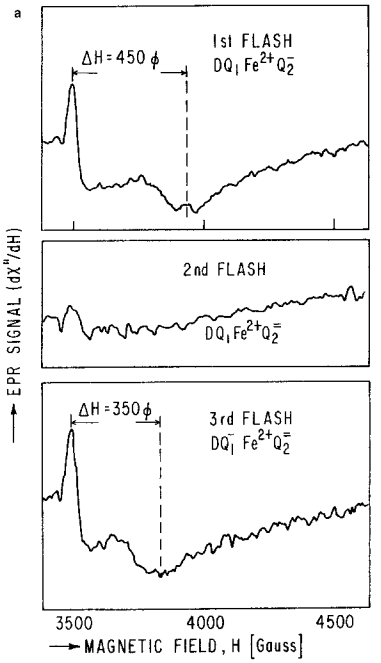

Fig. 6. a ESR signals of reduced quinone-iron acceptors of reaction centers of *Rps. sphaeroides* R-26 after 1, 2, or 3 laser flashes at room temperature in the presence of cyt *c* followed by rapid freezing [97]. *D* stands for the primary donor (Courtesy of Dr. G. Feher as reproduced in [1]). **b** Comparison of the ESR signal due to the primary acceptor of reaction centers of *Rps. sphaeroides* R-26 of which the iron was removed (left) and the ubiquinone anion radical (right) at 9.2 GHz and 34.9 GHz ($T = 1.3$ K). The $P860^+$ radical has been reduced with cytochrome *c* [92]

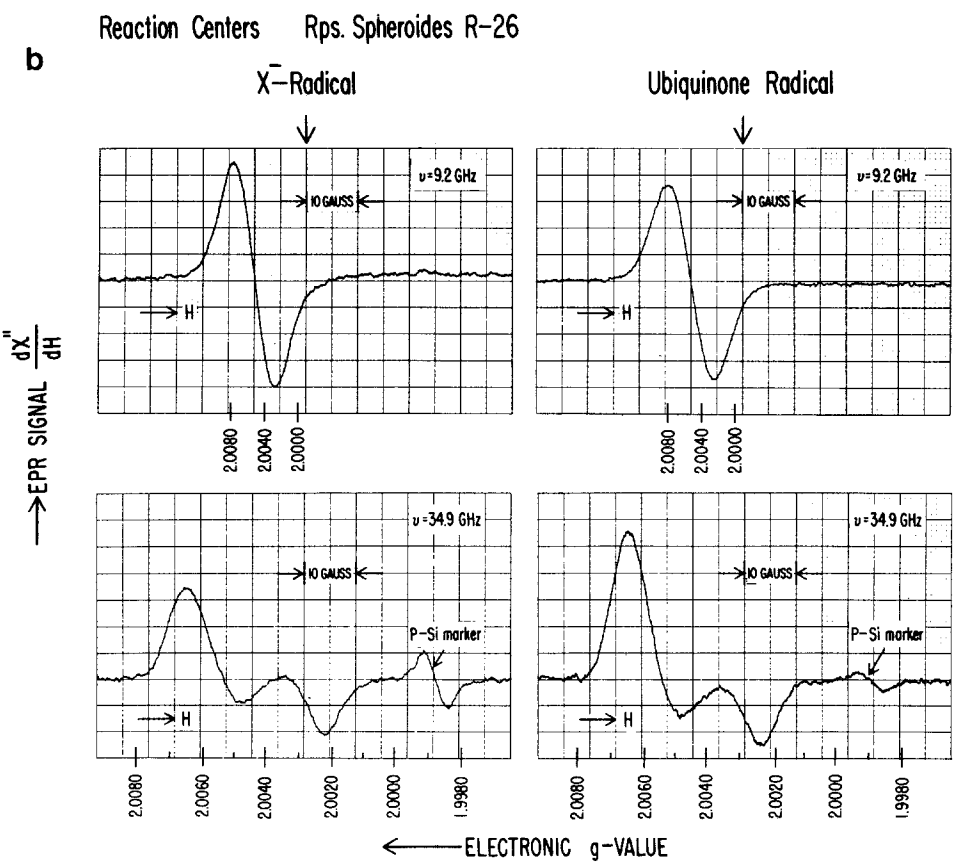

Fe does not take part in electron transport as an acceptor, but couples magnetically to the seminiquinone, thus shifting and broadening its ESR spectrum. The above evidence was corroborated by magnetic susceptibility measurements, which indicated that the magnetic moment of the reaction center (which is mainly due to the Fe) does not change upon photoreduction of the secondary acceptor [95]. From a study of the susceptibility as function of temperature, the magnitude of the exchange interaction between Q^- and Fe^{2+} was estimated to be -0.2 ± 0.1 cm^{-1} (about 2 kG) [95]. This is large on a magnetic resonance energy scale, but small on the scale of an optical spectrum, explaining that the latter is unperturbed by the iron.

From the reduced secondary acceptor uQ_1^-, the electron is transported to another quinone uQ_2, which serves as a two-electron gate to the rest of the electron transport chain. The shape and the apparent g-values (defined as baseline crossings of the derivative ESR signal) of the ESR signal of uQ_2^- Fe is somewhat different from that of uQ_1^- Fe, but the magnitude of the magnetic interaction is similar [96, 97, and Fig. 6a], suggesting that both quinones are close to the Fe (they are probably not liganded to Fe, as suggested by EXAFS studies [98]). It has been suggested that Fe acts as an 'iron wire' between uQ_1 and uQ_2, facilitating electron transport [99, 100]. This view received support from an experiment in which added uQ_2 could not be photoreduced in a purportedly iron-depleted photoactive subunit of the reaction center of *Rps. sphaeroides* R-26 [101]. It is, however, not excluded that the reaction center must be intact to provide a binding site (with or without Fe) for the uQ_2 [102], so that the function of the Fe remains conjectural.

Monitoring the ESR spectra of $u(m)Q_1^-$ Fe^{2+} and $u(m)Q_2^-$ Fe^{2+} as a function of redox potential has yielded information on the redox midpoint potential of the secondary and tertiary acceptors [77, 96, 106, 112, 123, 130]. The E_m of the secondary quinone-iron acceptors of the purple bacteria range between -130 and -200 mV at pK 6.5–9.8 depending on the species (see Table 2.3 of [1]). The E_m of F_1 of the gBPS is about -550 mV [76, 77].

Quinones have a slightly anisotropic g-value (e.g., for benzosemiquinone $g_x = 2.0065$, $g_y = 2.0053$, and $g_z = 2.0023$, with the x-axis along the carbonyl bands and the z-axis perpendicular to the molecule [103]). This made it possible to carry out an orientation study [104] of uQ_1 in reaction center particles from which the iron was removed according to [91]. The particles were suspended in an ethanolic phosphatidylcholine solution, dried on a quartz slide and illuminated in situ at 6 K. The ESR signal at $g \sim 2$ consists of a superposition of the lines of $P860^+$ and $uQ_{1(2)}^-$; the width of the composite signal proved to be a sensitive function of the angle between the slide and the magnetic field. *o*-phenanthroline, which blocks electron transport from uQ_1 to uQ_2, had no effect, suggesting that uQ_1 was reduced. Work on similar particles, employing the flash technique of [105, 106], indeed suggests that uQ_2 is lacking from particles prepared according to [91] ([107] and Gast, unpublished results). From the angular variation of the width of $P860^+$ uQ_1^- it was concluded that the x-, y-, and z-axis of uQ_1^- as defined above made a mean angle of 0°, 90°, and 90° with the normal to the plane of the membrane, with angular standard distribution of 40°.

Analogous studies were carried out on chemically reduced dried chromatophores. In these samples, illumination at 6 K produced the triplet state of the primary donor (see Sect. 6), whose ESR signal also showed strong angular variation, from which it was concluded that the dimer of P860 is oriented with the symmetry plane of the dimer (assumed to be composed of [nearly] parallel BChl molecules) approximately perpendicular to the plane of the membrane, in agreement with optical studies of P860 [108]. Hence, the secondary acceptor uQ_1 is oriented perpendicular to the dimer plane. If one adheres to the theory that electron transport mediated by uQ happens via the two carbonyl ends of the molecule, this seems to be a logical relative orientation. In vivo uQ_1 must be close to the surface of the membrane [109], and electron transport away from uQ_1 probably happens roughly parallel to the membrane (see, e.g., Fig. 4.3 of [36]).

Recently, ENDOR experiments have been carried out [110] on uQ_1^- of iron-depleted reaction center particles prepared according to [92]. Hf couplings of 1.2, 4.6, and 5.8 MHz could be discerned, in qualitative but not quantitative agreement with those obtained for uQ_1^- in vitro [111]. The difference may be due to a special environment of the quinone in vivo.

4.1.2 Green Bacteria, gPBS. As mentioned in the "Introduction", the green bacterial photosystem is basically different from that of purple bacteria. Like PS 1 but unlike the pBPS, the green photosynthesizing bacteria are capable of direct photoreduction of pyridine nucleotide. As this necessitates a fairly low potential of the secondary acceptor complex, this suggests that the gBPS acceptor system is more like that of PS 1 than like the pBPS. Indeed, early reports on membrane particles of *Chlorobium* indicated the presence of a Fe-S protein with $E_m \sim -550$ mV [113] and low-temperature photoreduction of a membrane bound iron-sulphur protein [77]. Recently, these observations have been amplified by optical and ESR experiments on reaction center preparations of the green sulphur metabolizing bacterium *Prosthecochloris aestuarii* [76]. Two distinct Fe-S centers were identified by ESR, which appear to function serially as secondary acceptors. The distal acceptor, which I will call F_2, with $E_m \sim -420$ mV, has principal g-values at 1.94 and 1.89 (at $g = 2.05$ a weak signal was observed, largely obscured by a background signal of the quartz dewar). The E_m and the spectrum of F_2 do not agree with the signal observed in [77]. The latter may have been due to a Rieske Fe-S type protein [78].

At $E_h \sim -450$ mV when F_2 is fully reduced, another acceptor, F_1, could be photoaccumulated when a fast electron donor was added to keep P840 reduced. The absorption difference spectrum showed a broad minimum at 445 nm. The ESR spectrum of F_1, obtained as a difference spectrum of samples frozen in the dark and in the light, showed a ferredoxin-like spectrum with g-values $g = 1.94$ and 1.88. The midpoint redox potential of F_1 was estimated to be ~ -560 mV; this acceptor appears to correspond to the ferredoxin compound observed earlier [113].

Even when F_1 was fully reduced by illumination at a redoxpotential of -420 mV before and during freezing, a strong triplet attributed to $P840^T$ was observed [75, 76]. This points to the presence of an acceptor antecedent to F_1. In

fact, an ESR signal at $g = 2$ could be accumulated by illumination with strong white light at $-5°$ C and during cooling to 80 K. The spectrum showed a symmetric Gaussian centered ag $g = 2.0040 \pm 0.0005$ with $\Delta H_{p\text{-}p} \sim 14$ G (measured at 5 K, at room temperature the width was 12.9 ± 0.3 G), indicative of a porphyrin monomeric anion radical (provissionally labeled *B*). The optical absorption difference spectrum of accumulated *B* strongly suggested that *B* is a BChl *a* monomer [246]. Surprisingly, illumination of the sample with accumulated *B*, i.e., in the state P840 $B^- F_1^- F_2^-$ still provoked the strong, spin-polarized triplet signal of $P840^T$. It was concluded that between P840 and *B* another acceptor must be located of as yet unknown identity. One may speculate that it is BPh *c*, a compound known to be present in the particles. This would reverse the order as suggested by Forman et al. [247] who proposed on the basis of the measured redox potentials in vitro that BChl *a* ($E_m = -0.86$ V in DMF) is the 'first' and BPh *c* ($E_m = -0.80$ V in DMF) the secondary acceptor.

4.2 The Secondary Acceptor Complex of Photosystem 1

The secondary acceptor of PS 1, where the negative charge gets stabilized after charge separation, consists of a complex of presumably three ferredoxin type iron-sulphur proteins (see for reviews [1, 114–116]). They are usually called *X*, *B*, and *A*, but in the interest of a unified nomenclature I will label them F_X, F_B, F_A. They are normally photoreduced in this order. That is, under ambient redox conditions, the first electron is stabilized on F_A ($E_m \sim -550$ mV [117]), the second turnover of PS 1 reduces F_B ($E_m \sim -585$ mV [117]) and the third may reduce F_X ($E_m \sim -730$ mV [58, 118]) if the back reaction $P700^+ X^- \rightarrow P700\, X$ is prevented by a strong reductant. In some organisms, the order of reduction of F_A and F_B may be inverted [119, 120], apparently due to modification of the midpoint redox potential of center F_B, which changed to -520 mV [120].

The ESR spectra of F_A^- in $F_B F_A^-$ and F_B^- in $F_B^- F_A^-$ are characteristic of ferredoxins with principal *g*-value at $g_x \sim 2.05$ (2.06), $g_y = 1.94$ (1.92), and $g_z = 1.86$ (1.89) (values between parentheses for F_B^-) (Fig. 7a, b). However, upon reduction of $F_B F_A^-$ to $F_B^- F_A^-$, the peak at $g = 1.86$ of F_A^- disappears and congeales with the peak at $g = 1.89$ attributed to F_B^-. Moreover, in preparations with solely F_B reduced, the principal *g*-values are 2.065 (2.072), 1.935 (1.932), and 1.882 (1.876), which change to 2.047 (2.072, 2.053); 1.941, 1.922 (1.940, 1.925); 1.887 (1.876, 1.844) when also F_A^- is reduced [119] ([120]). The disappearance or shifts of some features and the appearance of new ones when both F_A and F_B are reduced, points to a magnetic interaction between F_A^- and F_B^-, the nature of which is presently not understood.

The 'true' secondary acceptor, F_X, was first seen by McIntosh et al. [64] and Evans et al. [65, 67] in samples in which F_A and F_B were chemically reduced before freezing and which were illuminated at low temperature (note that ESR spectra of ferredoxins must be recorded at temperatures around 15 K because of the rapid spin-lattice relaxation; reduction is usually carried out at room temperature by some combination of chemical reductants and light, whereupon

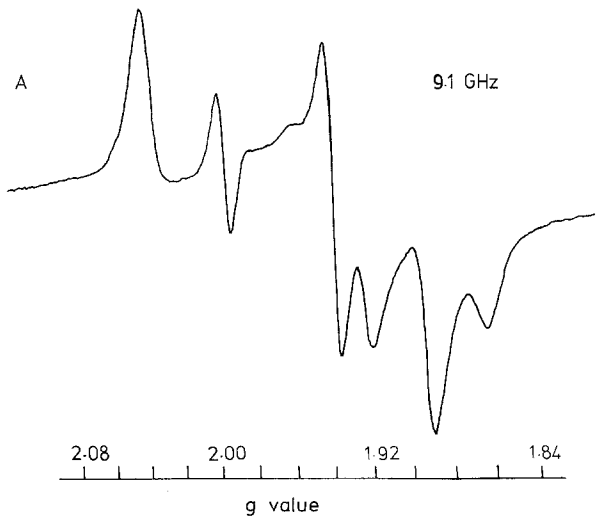

Fig. 7 A. Spectrum of the reduced PS 1 secondary acceptors F_A^- and F_B^- at 9.1 GHz ($T = 5$ K). PS 1 particles were reduced with 25 mM dithionite for 15 min in the dark and frozen under illumination. One aliquot was used for *X*-band, one for *K*-band spectrometry. Modulation amplitude: 20 G, microwave power: 20 mW. Incomplete reduction of F_B leaves part of the $g = 1.86$ line visible (from [1])

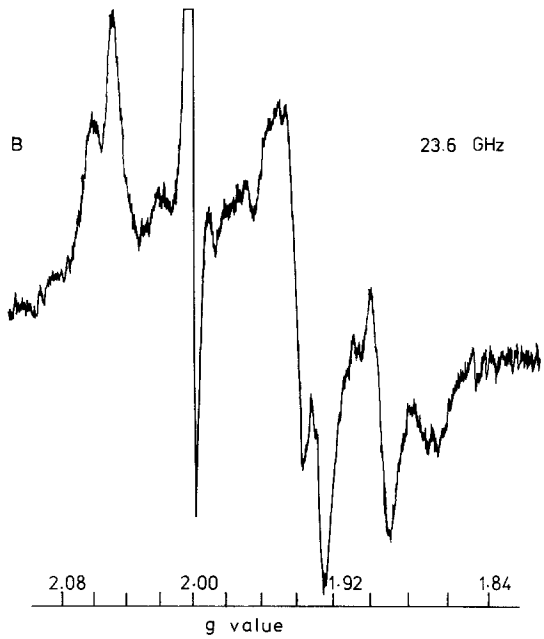

Fig. 7 B. Spectrum of F_A^- and F_B^- at 23.6 GHz (*K*-band) ($T = 1.5$ K). Modulation amplitude: 12 G, microwave power: 0.2 μW. Reduction as in Fig. 7a (from [1])

the samples are rapidly frozen). Its ESR spectrum resembles that of ferredoxins (Fig. 7c) but the *g*-values at $g \simeq 2.08$, 1.87, and 1.76 [67, 121, 122] are somewhat different. F_X^- can be accumulated by carrying out room temperature reduction at very low E_h (about −600 mV) under illumination, keeping the light on while freezing the sample [66, 121], or by strong illumination and freezing alone [122].

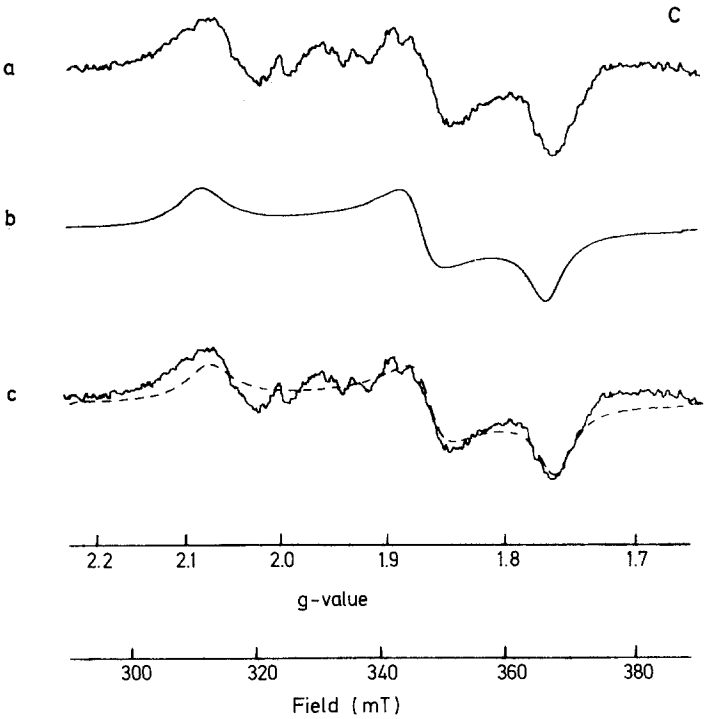

Fig. 7 C. Comparison of the experimental ESR spectrum of F_X^- with a computer-simulated spectrum **(a)** Difference spectrum of a sample with F_A and F_B reduced and a sample with F_A, F_B, and F_X reduced. Microwave power: 100 mW, modulation amplitude: 10 G, temperature: 10 K. **(b)** Simulated spectrum on the basis of Gaussian intrinsic lineshape. **(c)** Superposition of **(a)** and **(b)** (from [129])

At least one of the ferredoxins F_A, F_B, F_X gives rise to a weak optical absorption difference signal at 430 nm, a wavelength characteristic of ferredoxin reduction [115]. Although the midpoint redox potential of the signal, P430, was reported to be −470 mV [124], its appearance and disappearance corresponds closely to that of the ESR signal of the reduced acceptor F_A^-, as a result of a change in redox conditions [125] or of its physical removal [126].

The decay kinetics of F_A^-, F_B^-, F_X^- can be monitored optically at 430 nm, by ESR at low temperatures and by monitoring the decay of $P700^+$ at low temperature, when presumably only direct recombination of the charges on P700 and the acceptor complex is responsible for the decay. The decay rates are a complex function of temperature and redox potential [56, 58, 62–67, 127]; the reaction can be described as a tunneling process [59, 60, 128]. Photoproduction of $P^+F_XF_BF_A^-$ and $P^+F_XF_B^-F_A^-$ is irreversible at low temperature (below about 20 K); at 10 K $P^+F_X^-F_BF_A^-$ decays to $PF_XF_B^-F_A^-$ with a halftime of 0.7 s [64].

The exact nature of the complex $F_XF_BF_A$ is still poorly understood. It has been suggested that F_BF_A is a 4 Fe–4 S cluster [128], but this has not been corroborated by ESR spectroscopy at 24 GHz (Fig. 7b). The interaction between F_B^- and F_A^- indicated by the $g = 1.86 \rightarrow 1.89$, $g = 1.935\ (2) \rightarrow 1.922\ (5)$,

and $g = 2.065$ (72) $\rightarrow 2.047$ shifts does suggest that these two clusters are close; remarkably enough, reduction of F_X^- does not seem to entail much change in the $F_B^-F_A^-$ spectrum. The fact, that F_X, F_B and F_A are reduced roughly in a 1 : 1 : 1 ratio [50, 118, 129] suggests that all three are essential components in linear electron transport.

Orientation was achieved by alignment in a high magnetic field [122] or by drying chloroplasts on a quartz slide [131]. In the latter technique, illumination of dark adapted samples at cryogenic temperatures always provoked partial reduction of center F_B together with that of center F_A; more fully reduced F_B was obtained by preillumination before and during freezing. Center F_A ($g_X = 1.86$; $g_y = 1.94$; $g_z = 2.05$) was found to have the principal x- and y-axes of its g-tensor lying at an angle of about 40°, and the z-axis at about 25° to the membrane plane. For center F_B a certain ambiguity arose, because in the $g = 2.05$ region not two, but three peaks were resolved by the angular dependence of their intensity[3], at 2.04, 2.05, and 2.07. If one accepts the peaks at $g = 2.05$, 1.92, and 1.89 originating from center F_B as such, then its z- and x-axes are oriented in the plane of the membrane, while its y-axis is orthogonal to the plane. However, also the set 2.07, 1.94, and 1.89 allowed consistent interpretation of the angular dependence. The authors argued that the third g-value in the ~ 2.05 region could arise from a magnetic coupling between F_A^- and F_B^- which also causes the disappearance of the $g = 1.86$ peak of F_A^- upon reduction of F_B^-, and that also the new signal at 1.92 might be due to magnetic interaction, and not represent the proper principal value of a lone F_B^- cluster, in agreement with [119]. The disappearance of the 1.86 line of F_A^- is probably not due to a shift as the 1.89 peak of the $F_B^-F_A^-$ material does not show a mixed angular dependence, so that either the g_x-axis of F_A^- rotates to a position colinear with that of F_B^-, or the 1.89 feature is an entirely new phenomenon arising out of the interaction $F_B^-F_A^-$. Against the latter possibility argues the high frequency (24 GHz) experiment (Fig. 7d). From the work on magnetically oriented chloroplasts [122], center F_X was found to have its g_x-axis predominantly normal to the membrane, hence the g_y- and g_z-axes predominantly in the membrane plane.

The above experiments provide a valuable contribution to the study of the acceptor side of PS 1 but clearly further experimentation is needed to resolve the abstruse structure of the $F_XF_BF_A$ complex.

4.3 The Secondary Acceptor of Photosystem 2

Because of the required redox potential (two E_m values of about +0.03 and −0.25 V [134, 135], presumably due to heterogeneity of PS 2) Nature's 'logical' choice for the secondary acceptor of PS 2 would be a quinone. Indeed, Stiehl and Witt [136] and van Gorkom [137] established by optical absorption difference

3 In these studies with a relatively low degree of order, the observed ESR spectrum is a composite of many spectra with variable degree of order. The result is a spectrum resembling the powder spectrum, in which the 'turning point' lines show an angular dependence of their intensity but not of their position [132, 133]

spectroscopy that the secondary acceptor of PS 2 is a plastoquinone; in this article I will label it $pQ_1$to distinguish it from the bacterial acceptors (it is usually called Q for 'quencher', because its reduction enhances the yield of PS 2 fluorescence). pQ_1 acts as a one-electron acceptor, analogous to Q_1 in the pBPS. For a long time pQ_1^- eluded detection by ESR, and only recently the high yield preparation of PS 2 subchloroplast particles with ratio Chl/P680 ~ 40 has permitted its direct observation by ESR [138]. Its specrum shows a feature near $g = 1.82$ much resembling that of the spectrum of the pBPS secondary acceptor $uQ_1^- \cdot Fe^{2+}$; apparently pQ_1 is complexed to a transition metal, probably also an iron. When the ratio Fe^{2+}/P680 is lowered to 0.6 by treatment with chaotropic and complexing agents, an ESR signal at $g = 2.0044 \pm 0.0003$ and width $\Delta H_{p\text{-}p}$ ~ 9 G becomes visible [139, 140], very similar to the signal of uQ_1^- when Fe^{2+} is dissociated from the secondary acceptor in the pBPS (Sect. 4.1.1). The acceptor following pQ_1 is also a plastoquinone, it serves as a two-electron gate just as uQ_2 in the pBPS. As yet it has only been observed optically[4] [139, 140]; by analogy with the pBPS one may expect its singly-reduced form to have a spectrum similar to that of $uQ_2^- \cdot Fe^{2+}$.

5. The 'First' Electron Acceptors

The history of research on primary reactions shows that it is hazardous to speak of 'first' electron acceptors. Yet, there is now a large body of evidence that between the 'secondary' acceptors $u(m)Q_1$, F_1, pQ_1, and F_X, and the donors P860, P840, P680, and P700, respectively, an intermediate is located on which the electron resides for an appreciable time, in the order of 0.2 ns in the case of the pBPS, before traveling on to what I call in this review the secondary acceptor. Although there are some indications, that at least in the pBPS a very short living (~ 3 ps) transitory charge transfer state is produced before actual charge separation is effected, I will call the well-characterized intermediary acceptor, the 'first' acceptor (to avoid confusion with older and in my opinion now obsolete nomenclature in which $u(m)Q_1$, pQ_1, and F_X were called 'primary' acceptors, I will use 'first' instead of 'primary').

5.1 pBPS: Bacteriopheophytin, BPh

The presence of an acceptor earlier than $u(m)Q_1$ in the photosystem of the purple bacteria was first demonstrated by fast optical absorption difference spectroscopy [143]. In samples in which uQ_1 was prereduced a transient state with a lifetime of about 15 ns was observed, whose spectrum could be resolved in the sum of that of $P860^+$ and one that resembled much the absorption difference spectrum of monomeric BPh a – BPh a^- [144]. In samples at ambient redox

4 The acceptor following pQ_1 has two labels, B [141] and R [142]. In the interest of a uniform nomenclature one might call it pQ_2; alternatively one might fuse the two labels to the symbol ⊠, thus honouring the two discoverers and at the same time indicating the two-electron gate character

potential this intermediate was also observed, now with a lifetime of about 200 ps [145, 146]. In prereduced samples the transient state $P860^+$ BPh^- uQ_1^- decayed at room temperature for about 15% to the triplet state $P860^T$BPh uQ_1^- [143], the remainder to the ground state P860 BPh uQ_1^- (probably for a large part via the excited state P860* BPh uQ_1^- [147]). At low temperatures, below about 50 K, the yield of $P860^T$ approached unity [148]. (See for more information on the triplet state of the primary donors Sect. 6).

In most bacteria the acceptor BPh *a* proved difficult to reduce chemically, showing that its redox midpoint potential must be lower than −0.65 V [149]. However, in *Chromatium minutissimum* [150] and in *Chromatium vinosum* [151] a cytochrome *c* is able to irreversibly donate electrons to $P860^+$ at low temperature sufficiently fast that one can accumulate BPh a^- under conditions of strong illumination and low redox potential. This has permitted its study by ESR [150, 151]; the result confirmed the evidence from the optical spectra. Later, accumulation of BPh a^- under conditions of low redox potential and strong illumination was also obtained in isolated reaction centers of *Rps. sphaeroides* R-26 to which purified excess cyt *c* had been added [152]. Production of BPh b^- by (photo)chemical reduction in *Rps. viridis* (BChl/BPh *b* has a lower redox midpoint potential than BChl/BPh *a*) is accompanied by the loss of the triplet signal due to $P960^T$ [153, 154] as expected for BPh being the first 'stable' acceptor. From the disappearance of the triplet in *Rps. viridis* and concomitant appearance of BPh^- a redox midpoint potential of the couple BPh/BPh^- of ~ -400 mV was deduced. This value deviated from the value of −620 mV arrived at by optical titration [155], which discrepancy was attributed to poor equilibration of the redox couples and mediators [154]. However, this argument was based on a misunderstanding of the redox procedures employed (see, e.g., Fig. 3 and caption in [155]), so that presently the lower value of −620 mV is preferred (Klimov and Prince, private communication and [113]).

The ESR signal of BPh^- is composed of a Gaussian line at $g = 2.0036 \pm 0.0002$ [152, 156, 157] and linewidth ranging between 12−15 G, depending on conditions and species [150−159] and, under certain conditions, a doublet signal with splitting 65−200 G (see below). The low temperature ENDOR spectrum of the narrow signal of BPh^- *a* in reaction centers of *Rps. sphaeroides* R-26 [160] showed one splitting of 8−9 MHz, similar to that of BChl a^- and BPh a^- in vitro. The low temperature ENDOR spectrum of BPh^- *b* in reaction centers of *Rps. viridis* [156] showed splittings of 0.8, 7.8, and 9.0 (± 0.3) MHz. This compares with 2.0, 7.3, and 8.4 (± 0.3) MHz for BChl b^- and 8.7 ± 0.3 MHz for BPh b^- [156, 157]. Clearly, the ESR and ENDOR parameters (linewidth, *g*-value, hf splitting) do not permit to choose between BPh^- and $BChl^-$ as 'first' acceptor, but they do indicate that the species involved is a *monomer*. This agrees with the optical data, which strongly suggest that only *one* molecule is involved and that this molecule is bacteriopheophytin [150, 151, 161].

The doublet signal mentioned above was observed in *C. vinosum* where it appeared at temperatures below 15 K and at high microwave power [151, 159] (Fig. 8). It was also detected in chromatophores of *Rps. viridis* when BPh^- *b* was

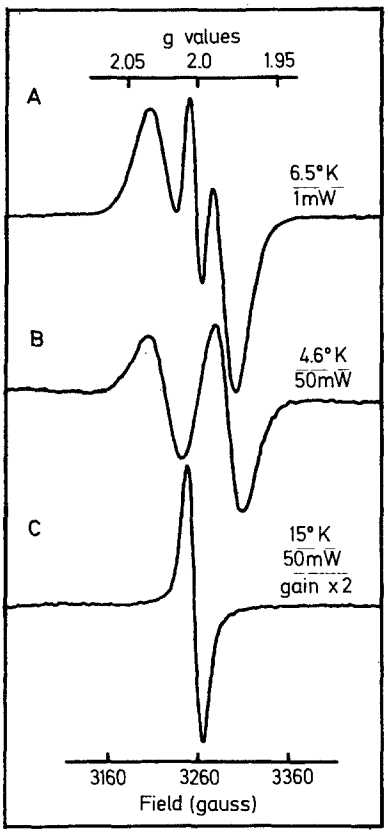

Fig. 8. ESR spectra of the reduced first acceptor BPh a^- in reaction centers of *C. vinosum*. Difference spectra of samples illuminated for 3 min at 200 K and non-illuminated samples. Modulation amplitude: 5 G, other settings as indicated [159]

trapped by illumination at −300 mV and 300 K, but not by trapping at 200 K [154]. The origin of the doublet was, by analogy to similar signals found in coenzyme B12 containing an organic radical interacting with a high spin cobalt atom [162], sought in an exchange interaction between BPh^- and Q_1^-. The splitting of the doublet showed a strong variation with pH [154], and in reaction centers it could also be induced at 200 K when LDAO, but not when SDS was present as detergent [154]. The latter result suggests that the magnetic interaction between *mQ* and Fe is necessary (Sect. 3.1) for the production of the doublet signal; see, however, below.

BPh^- *a* reduced in reaction centers of *Rps. sphaeroides* complemented with cyt *c* [152] showed only a narrow line, but when the native acceptor ubiquinone was extracted and substituted with menaquinone (which is the native acceptor in *C. vinosum* and *Rps. viridis*), a spectrum composed of the narrow and the broad, split, signal appeared. On the basis of the kinetics of formation and on data on the kinetics of reduction of the quinone acceptors as monitored optically, it was concluded that the narrow signal originates in reaction centers in which the secondary acceptor is *doubly* reduced and therefore diamagnetic, whereas the split signal is due to magnetic interaction between BPh^- and the singly reduced secondary acceptor. The difference between uQ_1 and mQ_1 resides in their rates

for double reduction, which differ by about two orders of magnitude ($k(uQ_1) = 10^2 \cdot s^{-1}$; $k(mQ_1) = 0.25\ s^{-1}$ [152]). Note, that these rates of double reduction are comparatively slow, so that under physiological conditions Q_1 is a strict one-electron gate.

Apparently, in reaction centers reconstituted with mQ a mixture of states P860 BPh^- mQ_1^- Fe^{2+} and P860 BPh^- $mQ_1^=$ Fe^{2+} is produced. Such mixtures might explain the various signals of BPh^- found earlier [151, 154, 158, 159], and especially the detergent and pH dependence is probably related to changes in the rate of double reduction of mQ_1.

In green bacteria, reduction of the 'first' acceptor has as yet not been possible, as judged by the continued photoproduction of the triplet state $P840^T$, even under strongly reducing conditions [76]. This is probably due to the difficulty of finding a suitably fast electron donor to $P840^+$.

5.2 PS 1

Some time after the discovery of F_X, in PS 1 subchloroplast particles under strongly reducing conditions [163], or stripped of the three ferredoxin-type acceptors $F_{X,B,A}$ by detergent [164] or heat treatment [165], a fast (7 μs) reversible decay of the optical absorption difference signal of $P700^+$ was observed. This fast decay was attributed to the back reaction between $P700^+$ and a photoreduced acceptor earlier than F_X. This acceptor cannot be a pheophytin *a* (Ph *a*), because this is reported to be lacking in PS 1 particles [166]. Also the E_m of the couple Ph *a*/Ph a^- (−0.64 V) is rather too high, although arguments based on in vitro redox midpoint potential should be used with circumspection (for example, the E_m of the couple P860 BPh/$P860^+BPh^-$ in the pBPS is only ~ 0.05 V higher than the energy of P860* and much lower than that of the couple BPh/BPh^- at −0.9 eV [147]. The difference spectrum of the fast $P700^+$ decay showed, when corrected for the difference spectrum of $P700^+$ formation, features characteristic for Chl *a* but not for Ph *a* reduction [165, 168]. In addition, the optical difference spectrum of a fast decaying component (1 ms) after a flash excitation of PS 1 particles at 5 K showed features attributed to reduction of a Chl *a dimer* [169, 170]. In contrast, the optical difference spectrum of the photoaccumulated reduced intermediate was very similar to that of monomeric Chl a^- reduction in vitro [168], so that the 1 ms component may have been due to a triplet state [1].

The question whether the acceptor between P700 and F_X is a Chl *a monomer* or *dimer* appears to be settled by ESR and ENDOR experiments on the photoaccumulated reduced acceptor in PS 1 particles [171–173]. A Gaussian [171], or somewhat asymmetric [172] line was observed at $g = 2.0037$ [172] or 2.0033 ± 0.0002 [173] of width $\Delta H_{p\text{-}p} = 13.3$ G [172], ~ 13 G [171] or 13.2–13.9 G [173]. The asymmetry was abolished by detergent treatment [172]. The *g*-value reported in [172] is out-of-line with that of Chl a^- in vitro (2.0029 [168]) and that found in [173]; the reason for this discrepancy is not clear.

Low-temperature ENDOR experiments (at 130 K) yielded two high-frequency resonances with hf coupling of 1.7 and 4.9 G [173]. Corresponding

resonances of Chl a^- in vitro which presumably are due to rotating methyl groups [168, 174] yield couplings of 1.95 and 4.05 G. This is fairly conclusive evidence that the 'first' acceptor of PS 1 is a Chl *a monomer,* not a *dimer.*

Recently, it has been reported that there is an antagonism between the PS 1 triplet state (see Sects. 4.4.1 and 6) and the appearance of the Chl a^- ESR signal [248]. This suggests that Chl *a* is, at least on a ns timescale, the first 'stable' acceptor.

5.3 PS 2

In analogy with *C. minutissimum* and *C. vinosum,* PS 2 of plants possesses a fast electron donor to $P680^+$, allowing photoaccumulation at low redox potential ($E_h < -200$ mV) of a reduced acceptor intermediate between P680 and pQ_1 [175]. Its optical absorption difference spectrum showed features attributed to pheophytin *a* (Ph *a*) reduction [144, 175]. This observation was corroborated [137] by the observation of a magnetic field-induced increase in fluorescence in the alga *Chlorella* analogous to the magnetic field effect on the fluorescence of bacteria [176]. The latter field effect is attributed to a field-dependent rate of the back reacton $B860^+BPh^- \rightarrow P860^*BPh$, where P860* is the excited singlet state of the primary donor. The redox potential of Ph *a*/Ph a^- in vivo is -0.61 V [177, 178], which agrees well with the corresponding value in vitro, -0.64 V [168].

PS 2 particles which were photoreduced at 296 K at a potential of -450 mV showed an ESR signal with characteristics analogous to that of monomeric BPh^- of the pBPS, viz. $g = 2.0033 \pm 0.0003$, $\Delta H_{p\text{-}p} = 12.6$ B; 0.3 G [139, 179]. Photoreduction at 220 K resulted in a mixed ESR signal. At 6 K, a singlet *and* a doublet with splitting $\sim 52-55$ G is observed, the doublet disappearing above 15 K [140, 179]. When pQ_1 was extracted from lyophilized PS 2 particles with an organic solvent and the sample photoreduced at 220 K, only the singlet was visible at 6 K. These observations are very similar to those seen in the pBPS when BPh^- is trapped (see Sect. 4.1.1) and suggest that Ph a^- has an exchange interaction of $\sim$ 52 G with pQ_1^-.

Interestingly, when the PS 2 particles were treated with a chaotropic agent (0.55 M $LiClO_4$) plus 2–5 mM of the complexing agent *o*-phenanthroline which reduced the non-heme iron content to $\sim$ 0.6 Fe/P680, the doublet ESR signal was eliminated [140]. It could be restored with addition of 0.2 mM Fe^{2+}. When the iron was extracted an ESR line at $g = 2.0044 \pm 0.0003$ with width $\Delta H_{p\text{-}p} = 9.2 \pm 0.5$ G was observed [140]. This line was seen earlier in PS 2 particles [139], but not assigned. As it is not observed in particles extracted with an organic solvent [140], by analogy with the pBPS it is probably due to plastoquinone magnetically uncoupled from the high-spin iron.

The fact that the iron is necessary for the doublet signal is consistent with the theory of the magnetic exchange interaction between an organic radical and a high-spin Co^{2+} [162], which interaction also gives rise to a doublet signal with unequal amplitude of the high and low field lines. Applying the theoretical treatment of [162] to the doublet signal one would estimate that the $pQ_1^- \cdot Fe^{2+}$

complex has a g-value of $\sim$ 1.8, in nice agreement with recent observation [138].

The presence of singlet and doublet ESR signals in one preparation is, also by analogy with the pBPS, explained by assuming partial double reduction of $pQ_1 \cdot Fe^{2+}$ under strong illumination at low redox potential.

The above work was complemented by proton ENDOR experiments [173] at 130 K. Two high frequency resonances were observed with hf couplings of 4.60 and $\sim$ 12.3 MHz, respectively. These resonances are presumably due to rotating methyl groups; corresponding ENDOR resonances of monomeric Ph a^- and Chl a^- in vitro yield hf couplings of 5.5, 10.5 MHz and 5.5, 11.3 MHz, respectively. The agreement strongly supports the notion that the 'first' acceptor of PS 2 is a *monomeric* chlorophyllous species.

Recent experiments suggested an antagonism between the formation of the triplet state $P680^T$ and reduction of the acceptor Ph a, indicating that Ph a is the first 'stable' acceptor [178].

6. Triplet States of Primary Donors

When the secondary acceptor in any photosystem is prereduced, i.e., the reaction center is in the state PIX^-, illumination generates the radical pair state $P^+I^-X^-$. Recombination of the charges on P and I then may lead to the states PIX^-, P^*IX^- and P^TIX^-, in which P^* and P^T denote the excited singlet and triplet states of P, respectively. These reactions have been studied in detail in the pBPS by optical spectroscopy (absorption difference, fluorescence) [42, 147, 180, 181]. Likely, at room temperature the back reaction to P^* predominates over that to P, because strong delayed fluorescence with a lifetime similar to that of the radical pair P^+I^- is observed [150, 182–184]. P^T in the pBPS has a yield at room temperature of about 15% [185]. At low temperatures ($T < \sim$ 50 K), however, P^T is formed with a quantum yield of almost unity at 8 K [185, 148], and is easily observable by ESR as will be reviewed in this section.

6.1 p- and gBPS

Triplet ESR signals in reaction centers of purple bacteria were first observed by Dutton et al. [186]. It was quickly noted that the signals were spin-polarized, i.e., the intensity of the line deviated from Boltzman equilibrium, some of them even being emissive [187] (Fig. 9a). The pattern of spin-polarization is unusual. It cannot be obtained by intersystem crossing in a single molecule [188], but it is easily explained by the radical pair recombination reaction [189]: the radical pair is created from a singlet state, hence its total magnetization is zero, and remains zero during the short lifetime of the pair because of conservation of angular momentum. This means that spin dephasing can only lead to the formation of the $m_s = 0$ triplet state of the radical pair. Recombination then leads to populating the $m_s = 0$ triplet state of P^T in proportion to the amount of triplet character of the radical pair (for a discussion of spin dephasing in the radical pair, see e.g., [1,

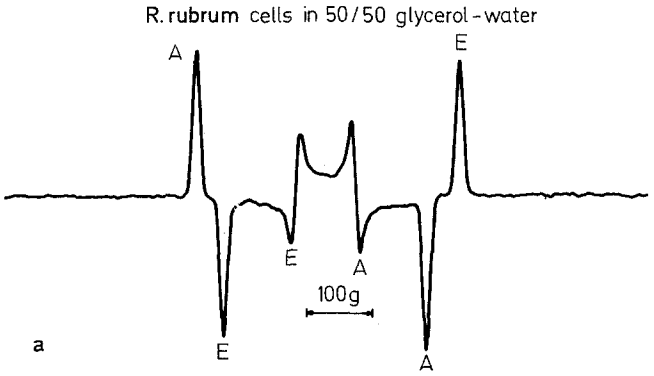

Fig. 9 a. Triplet spectrum of $P860^T$ in whole cells of *R. rubrum* in glycerol/water (1 : 1) at 5–20 K. The spectrum was recorded using a combination of field and light modulation [167]

42, 190]). It follows that the transitions $|T_0> \rightarrow |T_{+1}>$ and $|T_0> \rightarrow |T_{-1}>$ are absorptively and emissively polarized, respectively. The amount of polarization is large (ideally, the $|T_{\pm 1}>$ levels are completely empty), rendering the triplet easily observable.

The zero field splitting parameters of $P860^T$ lie in the range $|D| = 183-189 \times 10^{-4}\,cm^{-1}$ and $|E| = 31-35 \times 10^{-4}\,cm^{-1}$ compared to BChl *a* in vitro: $|D| \sim 238 \times 10^{-4}$, $|E| \sim 60 \times 10^{-4}\,cm^{-1}$ [191–193]; they are remarkably constant for the various BChl *a* containing purple bacteria investigated [1, 42, 194]. They are about 20% lower than those of BChl *a* in vitro, presumably due to the fact that P860 is a dimer. Also the molcular decay rates k from the triplet sublevels, $|T_0>$, $|T_{\pm 1}>$ in high field [195, 196], $|T_{x,y,z}>$ in zero magnetic field[5] [197, 198] (values of $k_{x,y}$ quoted in [199, 200] are almost certainly in error [1, 13, 42, 195, 196, 201]) deviate considerably from those of Chl^T in vitro (Table 2). Although it has been suggested that from a comparison between the in vivo and the in vitro values of $|D|$, $|E|$ and $k_{x,y,z}$ information can be obtained on the geometry of the two BChl macrocycles of the dimer [193], a reconsideration of the experimental data shows that presently this cannot be done, on account of the large values of the molecular decay rates k_x, k_y in vivo [1, 42, 198, 202]. Presumably, other contributions than those arising from purely geometric averaging, are responsible for the reduction of $|D|$ and $|E|$ and the large increase of $k_{x,y}$ of $P860^T$ with respect to $BChl^T$ in vivo. One such contribution is charge transfer, i.e., the triplet state $P860^T$ has some ($BChl^+ \cdot BChl^-$) character. Admixing as little as 5% of charge transfer character is probably sufficient to explain the reduction of $|D|$ [204]; it may

5 The triplet state can be observed in zero magnetic field by optically (fluorescence) detected magnetic resonance (ODMR, FDMR) between the $T_{x,y,z}$ sublevels that are split by the dipole-dipole interaction (Fig. 9b). With this technique very accurate values of $|D|$ and $|E|$ can be obtained, and with proper precautions, also precise values for the molecular decay rates $k_{x,y,z}$. See for a comprehensive introduction to ODMR [203], for its application to the reaction center chapter 9 of same [42]

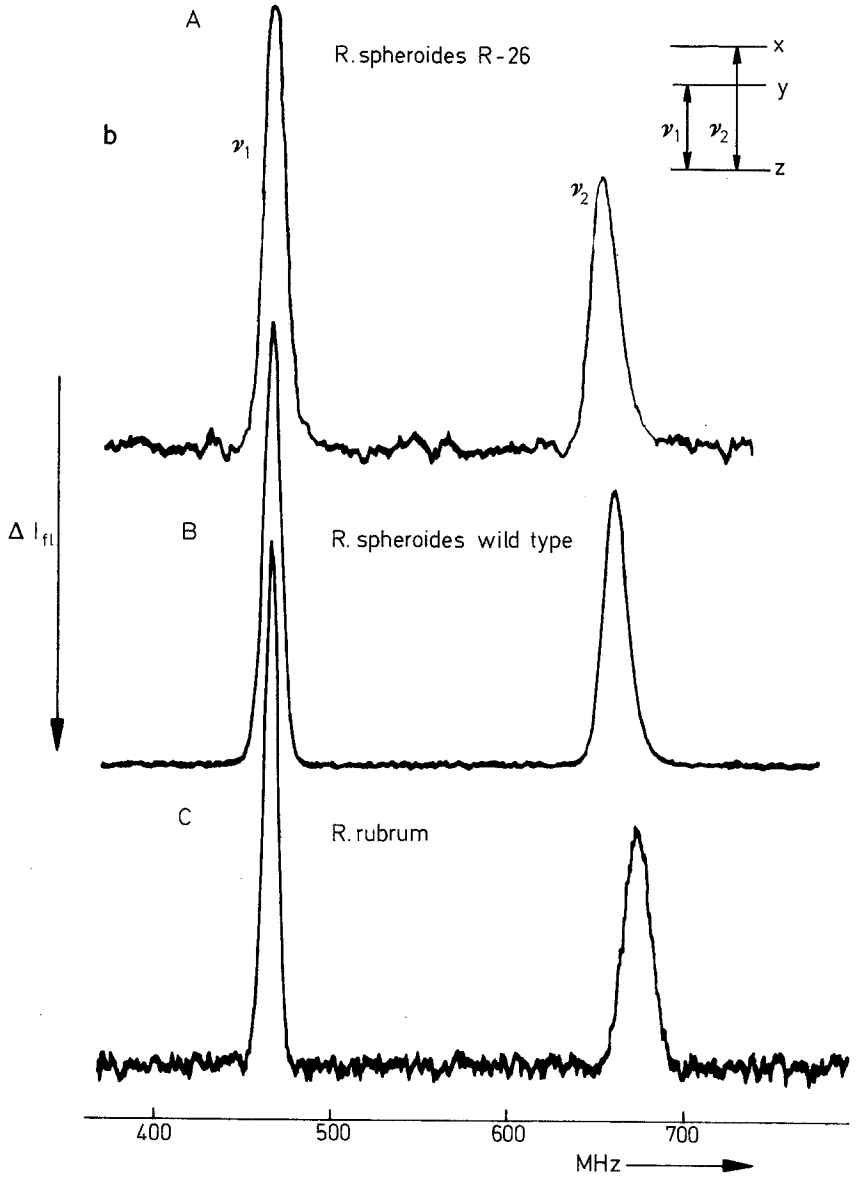

Fig. 9 b. Fluorescence-detected zero field resonance spectrum at 2 K of (A) *Rps. sphaeroides R-26, (B) Rps. sphaeroides* strain 2.4.1, and (C) *R. rubrum* strain S 1. Inset: the triplet sublevels in zero magnetic field, split by the dipole-dipole interaction. Frequencies ν_1 and ν_2 are given by $(|D|-|E|)/h$ and $(|D| + |E|)/h$, respectively, with $|D|$ and $|E|$ the zero field splitting parameters. Continuous irradiation with blue light, detection at 911 nm using amplitude modulation of the microwaves and lock-in detection. The spectra are single scans [197]

Table 2a. Zero field splitting parameters ($cm^{-1} \times 10^4$) of the triplet state of chlorophylls in vivo and in vitro[a]

Species	$\|D\|$	$\|E\|$	Reference
Rps. sphaeroides 2.4.1	185.9 ± 0.6	32.4 ± 0.3	[198]
centers[e] R-26	187.2 ± 0.2	31.2 ± 0.2	[197]
Reaction centers[e] R-26	188.3 ± 0.4[e]	32.0 ± 0.4[e]	
R. rubrum S1	187.8 ± 0.6	34.3 ± 0.3	[198]
Rps. gelatinosa 8290	185.5 ± 0.6	32.3 ± 0.3	[198]
Rps. capsulata ATC 23872	184.2 ± 0.6	30.3 ± 0.3	[198]
Rps. palustris 2.1.6	184	32	[153]
	183 ± 2	35 ± 2	[211]
Rps. viridis cells	157	37	[153]
	153 ± 2	37 ± 2	[211]
	156.4 ± 0.5[e]	37.9 ± 0.5[e]	
Reaction centers[e]	159.0 ± 0.4[e]	40.0 ± 0.4[e]	
C. vinosum D	177.4 ± 0.6	33.7 ± 0.3	[198]
T. pfennigii 9111	158	39	[158]
P. aestuarii	207 ± 2	37	[75]
PS 1 particles	278 ± 9	39 ± 9	[213]
	283	40	[248]
PS 2 particles	290	44	[248]
BChl *a*[b]	238 ± 5	69 ± 3	[193]
BChl *a*[c]	226 ± 5	59 ± 5	[191]
BChl *b*[d]	216 ± 6	55 ± 2	[192]
Chl *a*[c]	281 ± 6	39 ± 3	[245]
Chl *b*[c]	289 ± 4	49 ± 3	[245]

[a] The sign of D of the chlorophylls in vitro is positive [208]
[b] ^{1}H-THF
[c] ^{1}H-methyl THF
[d] ^{1}H-toluene + 10–15% pyridine
[e] FDMR experiments (H. J. den Blanken, private communication)

Table 2b. Sublevel decay rates in s^{-1} for the bacterial triplet state

Species	k_x	k_y	k_z	Reference
Rps. sphaeroides 2.4.1	10,500 (700)	9,200 (700)	1,900 (100)	[197, 198]
R-26	9,000 (1,000)	8,000 (1,000)	1,400 (200)	[197]
Reaction centers R-26	8,250	8,250	1,280	[185]
R. rubrum	8,000 (700)	7,200 (700)	1,350 (150)	[197, 198]
Rps. viridis reaction centers[a]	13,800 (1000)	16,100 (1000)	2,420 (100)	
P. aestuarii	3,000 (400)	3,000 (400)	1,300 (150)	[75]
BChl *a*	2,287 (280)	3,321 (572)	661 (74)	[200]

[a] FDMR results (H. J. den Blanken, personal communication)

have a drastic effect on the decay rates [205, 206]. For other possible contributions see [42].

The $|D|$ and $|E|$ values of the BChl *a* containing species *C. vinosum* and the BChl *b* containing *Rps. viridis* deviate from the values quoted above, being $|D| = 117.4$, $|E| = 33.7$ [198], and $|D| = 157$, $|E| = 37 \times 10^{-4}$ cm^{-1} [153], respectively. The latter values should be compared to those of

BChl *b* in vitro, viz. $|D| = 212 \pm 6$, $|E| = 55 \pm 2 \times 10^{-4}\,cm^{-1}$ [192]. Thus, for the two species the $|D|$ values are about 25% lower than the $|D|$ of the chromophore in vitro, instead of the more generally found reduction of 20%.

The decay rates of *Rps. viridis* (Table 2b) deviate considerably from those found in the BChl *a* containing purple bacteria. This might be related to a somewhat different geometry of the primary donor (see Sect. 3.1). In passing we note, that to study $P960^T$ care should be taken to avoid photoreducing the 'first' acceptor BPh *b* in *Rps. viridis* at the low redox potentials employed for reduction of mQ_1. Even at 4 K, cyt *c* donates sufficiently rapidly to $P960^+$ to photoaccumulate BPh^- in a few minutes. Hence, one should work under conditions that cyt *c* is oxidized [153, 154].

Also in the gPBS a reaction center triplet state has been observed [74, 75]. The zero field splitting parameters were $|D| = 207 \pm 2$ and $|E| = 37 \pm 1 \times 10^{-4}\,cm^{-1}$, i.e., rather different from those found in the pBPS. Also the decay rates deviated considerably (Table 2b). Apparently, the topology of P840 (which presumably is also a BChl *a* dimer, Sect. 3.2) of *Prosthecochloris aestuarii* is different from that P860, but it is as yet too early to draw conclusions with regard to the nature of the difference.

By virtue of the strong anisotropy of the triplet transitions, the triplet state is a very useful probe of the geometry of the primary donor. The technique of magnetophotoselection combines the magnetic anisotropy with the anisotropic absorption of polarized light, and yields information on the orientation of the triplet spin axes relative to optical transition moments of the pigments [207–210]. Alternatively, the photosynthetic membranes themselves may be oriented (by freezing in a high magnetic field, or by drying on a quartz slide) and the ESR spectrum recorded as a function of the angle between the plane of the membrane and the magnetic field [104, 211].

The magnetophotoselection study of [210] [the analysis presented in [209] suffers from the unjustified assumption that the polarization is not angle-dependent (it is, because the decay rates $k_{(0,\pm1)}$ from the high field triplet levels depend on the angle between the magnetic field and the spin axes); also the interpretation of the optical spectrum of reaction centers of *Rps. sphaeroides* R-26 is not clear (Fig. 3 of [209])] yields the angles between the spin axes and the Q_y transition moment of the primary donor $(BChl\,a)_2$ (at 870 nm) and the Q_x transition of one of the associated bacteriopheopytins (at 546 nm). The angle between the two quoted transition moments is about 60°, in good agreement with linear dichroism studies [212]. Moreover, the decay rates $k_{x,y,z}$ resulting from the computer fits to the oriented triplet spectra confirmed those resulting from the zero field resonance work in Leiden [197, 198].

From studies on the reaction center triplet in magnetically oriented membranes of *Rps. viridis* and *R. palustris* the angles which the spin axes make with the normal to the membrane could be determined. They are about 45°, 45°, and 80° for the *x*, *y*, and *z* spin axes, respectively [211]. The angles differ from those reported in [106] for reaction centers oriented in a phospholipid multilayer, viz. the spin *x*-axis nearly parallel to the membrane and the *y*, *z*-axes tilted 10–20° from the normal to the membrane. Apparently, the reaction center

protein orientes itself differently in artificial multilayer membranes and in the in vivo chromatophore membrane.

To conclude this section: although the triplet state of the primary donor is not an intermediate in the photosynthetic process under physiological conditions ('open' reaction centers), it is a versatile probe of the molecular architecture of the reaction center and of the redox reactions after initial charge separation. Its continued study by ESR and zero field resonance will contribute significantly to our understanding of the basic mechanism of photosynthesis.

6.2 PS 1 and PS 2

Quite recently, spin-polarized triplet states analogous to those found in he PBS were observed in PS 1 and PS 2 in subchloroplast particles in which the secondary acceptor was prereduced or removed [178, 213, 214, 248, 249]. Evidently, in the plant photosystem too, recombination of the charges on the primary donor and the first acceptor at low temperature may lead to a '$m_s = 0$' spin-polarized triplet state, fitting in nicely with the idea that the bacterial photosystem is a paradigm for all photosynthetic primary reactions. However, in both cases the $|D|$ and $|E|$ values were close to those of monomeric Chl a^T in vitro (Table 2). For PS 2 this would be in line with the suggestion that P680 is a monomeric Chl *a* molecule [71]. For PS 1 it could be due to the special pair being strictly parallel or to another prevailing mechanism of electron-hole recombination. As pointed out by Holten et al. [215], return of an electron from the reduced intermediary acceptor to the oxidized donor could operate not from the highest occupied molecular orbital (HOMO), but from HOMO − 1. The donor is then rereduced to the singlet state, while the intermediate (possibly a monomeric Chl *a* in PS 1) is left in the triplet state. Although it seems too early to assess whether in plants this process is thermodynamically favoured above the commonly received mechanism of recombination from the HOMO such as found in bacteria, it is an attractive concept worthy of further investigation. Alternatively, the contention that P700 is really a monomeric Chl *a enol* [68] is more than conjectural.

7. Polarized ESR Signals of Doublet States

A field presently in rapid development is research on photoinduced spin-polarized ESR signals originating from doublet states in the reaction center. The first such signal was observed in chloroplasts by Blankenship et al. [216], later work comprised other plant and algal preparations [217–224] and the pBPS [107, 225, 226]; see for recent reviews [1, 227]. After the first demonstration [225] that (in the pBPS) the polarized ESR signal could not be explained when a triplet state was assumed to be the precursor state of charge separation as suggested in [216, 217] for PS 1, 2, it is now generally accepted that the observed polarized signals in all photosystems arise because of the so-called radical pair mechanism, i.e., spin dephasing of two radicals having a finite exchange interaction, with charge separation from an excited singlet state.

The exact nature of the polarized signals in the plant system is as yet somewhat controversial [217, 218, 222–224] and it seems too early to evaluate the significance of these data for, e.g., the assignment of the first electron acceptor in PS 1 [218, 223]. It is clear, however, that potentially the study of polarized ESR signals is a powerful tool to probe the structure of the reaction center.

For the pBPS the situation seems to be somewhat clearer. In isolated reaction centers of *Rps. sphaeroides* 2.4.1 in the state P860 BPh uQ_1 with the iron uncoupled from uQ_1 by detergent treatment, the polarized ESR spectrum can be rather well explained assuming development of polarization in the initial radical pair $P860^+$ BPh^- followed by electron transfer to uQ_1^-, generating the polarized state $P860^+$ BPh uQ_1^- [225, 228]. In reaction centers with intact quinone-iron complex, no polarization was observed.

In reaction centers with prereduced secondary acceptor, i.e., in the state P860 BPh uQ_1^- (again no magnetic interaction between uQ_1 and Fe^{2+}), flash *or* continuous illumination resulted in the dark signal of uQ_1^- turning emissive [107] (Fig. 10a, b). This was well explained by assuming that the transient polarization of BPh^- could be transferred by exchange interaction to uQ_1^-. The cycle P860 BPh $uQ_1^- \overset{h\nu}{\rightarrow}$ $P860^+$ BPh^-_{pol} $uQ_1^- \rightleftarrows$ $P860^+$ BPh^-_{pol} $uQ_{1\,pol}^- \rightarrow$ $P860^T$ BPh $uQ_{1\,pol}^- \rightarrow$ P860 BPh $uQ_{1\,pol}^- \overset{h\nu}{\rightarrow}$ etc. then pumps polarization into $uQ_{1\,pol}^-$, the steady state amplitude of which will depend on light intensity in the case of continuous illumination, on microwave power and on temperature (because of spin-lattice relaxation) in a predictable fashion. The predictions were accurately verified by the experimental results [107, 226, 229]. With the aid of the model of exchange-mediated transfer of polarization and a simple calculation of the production of spin polarization in BPh^-, values for the exchange interaction between BPh^- and uQ_1^-, and between $P860^+$ and BPh^-, of ~ 3.5 G and 1–5 G were derived [107, 226]. The former agreed well with the value derived by Okamura et al. [152] from their experiments on the rate of electron transport from BPh^- to uQ_1^-. The latter exchange interaction has as yet not been verified by other methods, as the lifetime of the pair $P860^+$ BPh^- is only ~ 15 ns. The interaction is several orders of magnitude too low to explain the very rapid charge separation (~ 3 ps) [36, 230]. This was taken as an indication that to facilitate electron transport between $P860^+$ and BPh^-, an intermediary (charge transfer) state, possibly involving one or more of the accessory reaction center pigments, existed. Recent experiments with sub-picosecond flash excitation are in line with this expectation [231, 232].

In the past few years the electron spin echo (ESE) technique has found growing application in the study of photosynthetic material. Although the first electron spin echo resonance measurements date back to the early sixties [233, 234], the advent of fast microwave switches of moderate cost combined with high power pulsed microwave amplifiers has brought the technique out of the specialist's laboratory. Its advantages above conventional cw ESR are numerous: time response less than 0.1 μs, probe time a few ns, freedom of saturation phenomena, no field modulation, hence sensitive to broad signals, easier discrimination of signals with different spin-lattice (T_1) or spin-spin relaxation time (T_2), uncomplicated measurement of T_1 and T_2, possibility of

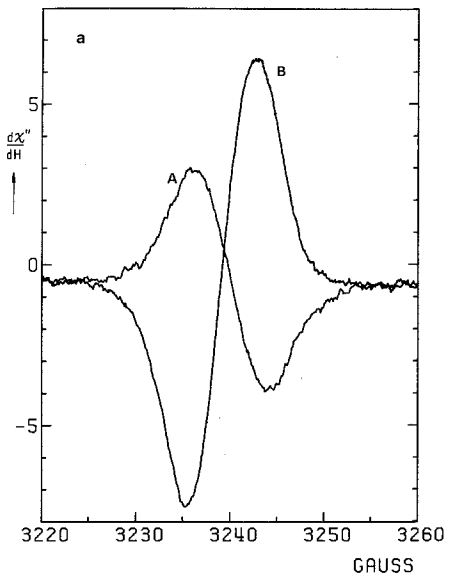

Fig. 10 a. *(A)* Dark ESR signal at 9.1 GHz and 5 K or reaction center particles of *Rps. sphaeroides* 2.4.1 in which the iron was uncoupled from the secondary acceptor uQ_1 by SDS treatment. uQ_1 was reduced by freezing under illumination in the presence of ascorbate (about 10 mM). *(B)* The emissive ESR signal that arises when the sample prepared as in *A*, is illuminated with white light at 5 K. Microwave power: 2×10^{-5} W, modulation amplitude: 5 G [107]

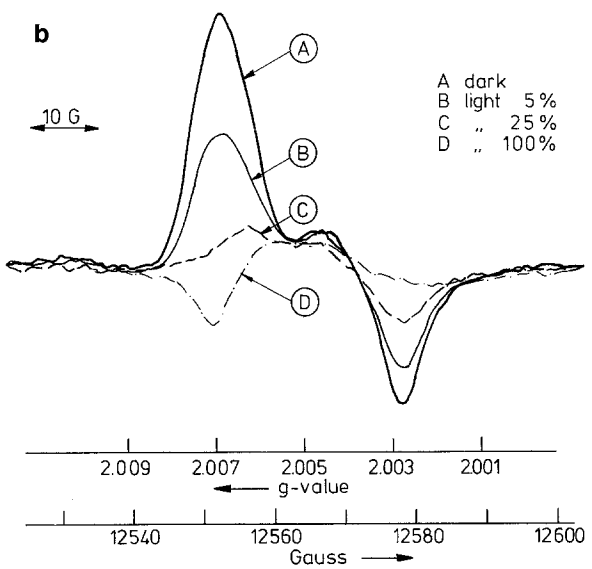

Fig. 10 b. ESR spectra at 35 GHz (Q-band) and 2 K of reaction center particles of *Rps. sphaeroides* 2.4.1. Sample preparation as in Fig. 10a. Spectrum *A* is recorded in the dark, spectra *B*–*D* in the light with relative intensity as indicated. The shape of *A* corresponds to that of uQ_1^- in Fig. 6b, illumination with increasing intensity leads to a spin-polarized, partially emissive signal (*B*–*D*) [241]

determining hf couplings by Fourier transform of the echo decay envelope, possibility of highly sensitive ENDOR employing the three-pulse-stimulated echo technique, etc.

Its usefulness has been demonstrated in the study of primary [52, 235–237] and secondary reactions in chloroplasts [238]. It was shown that $P700^+$ formation happens in less than 40 ns [52, 235] and an estimate of nitrogen hf and quadrupole couplings of Chl a^+ was made using the Fourier transform method

[52]. From a phase shift during the early spin-polarized stages of $P700^+$ formation it was concluded [236] that during the pulse sequence, i.e., within 100–200 ns after a 5 ns laser flash, $P700^+$ is magnetically interacting with another radical species, possibly the reduced 'first' electron acceptor Chl a^-.

In the pBPS, ESE was used to investigate spin-polarization transfer from BPh^- to uQ_1^- [229, 239]. Substantiating earlier assumptions [107, 226], it was demonstrated that the photoinduced emissive signal originates from uQ_1^-.

By employing ESE, T_2 of fully protonated and perdeuterated $P860^+$ were compared [240]. From the absence of an isotope effect it was concluded that electron hopping between the two BChl *a* molecules making up P860 was either very slow, or faster than a few ps. Inview of the evidence for electron sharing at a frequency exceeding 20 MHz (Sect. 3.1), the above experiment suggests that the two BChl's are strongly coupled and form a 'supermolecule', in line with the generally accepted interpretation of the optical absorption spectrum of isolated bacterial reaction centers (see, e.g., [36]).

Without doubt, the application of ESE in photosynthesis in only beginning, and in the next few years it will almost certainly provide us with new information on the early stages of charge separation by probing the spin memory of primary radicals.

8. Conclusions

This article aimed at a unified presentation of the primary photosynthetic reactions as probed by electron spin resonance. It is now fairly certain that the four photosystems now known to exist (PS 1, PS 2 in plants, pBPS and gBPS in purple and green photosynthesizing bacteria, respectively), all employ the same basic sequence of primary donor, transient 'first' acceptor, secondary, quasi-stable acceptor, etc. ESR has been of considerable help in the identification of the reactants, and it is of growing importance as a probe of the interactions between the reactants. ENDOR and triplet state ESR offers detailed, if still not fully interpreted, information on the molecular structure of the primary donor, whereas the youngest shoot, ESE, is of great promise for the study of polarized ESR signals which function as a spin memory of the much earlier event of primary charge separation.

The integrated utilization of optical and magnetic resonance techniques on photosynthetic preparations has proved to be very fruitful in the past, and I believe such integration will continue to be eminently useful in our efforts to unravel the primary processes in photosynthesis.

References

1. Hoff AJ (1979) Phys Rep 54: 75–200
2. Trebst A, Avron M (1977) Encyclopedia of plant physiology new series, vol 5: Photosynthesis I, Springer, Berlin Heidelberg New York
3. Duysens LNM (1952) Transfer of excitation energy in photosynthesis. Thesis, University of Utrecht

4. Duysens LNM (1954) Nature 173: 692–693
5. Goedheer JC (1958) Brookhaven Symp Biol 11: 325–331
6. Fuhrop JH, Mauzerall D (1969) J Am Chem Soc 91: 4174–4181
7. Commoner B, Heise JJ, Townsend J (1956) Proc Natl Acad Sci USA 42: 710–718
8. Sogo P, Jost M, Calvin M (1959) Radiat Res (Suppl) 1: 511
9. Loach PA, Walsh K (1969) Biochemistry 8: 1908–1912
10. Bolton JR, Clayton RK, Reed DW (1969) Photochem Photobiol 9: 209–218
11. Loach PA, Sekura DL (1968) Biochemistry 7: 2642–2649
12. Wraight CA, Clayton RK (1973) Biochim Biophys Acta 333: 246–260
13. Mushlin RA, Gast P, Hoff AJ (unpublished results)
14. McElroy JD, Feher G, Mauzerall DC (1969) Biochim Biophys Acta 172: 180–183
15. Corker GA, Sharpe SA (1974) Photochem Photobiol 19: 453–455
16. Schleyer H (1968) Biochim Biophys Acta 153: 427–447
17. Ruby RH, Kuntz ID, Calvin M (1964) Proc Natl Acad Sci USA 51: 515–520
18. Clayton RK, Sistrom WR (1966) Photochem Photobiol 5: 661–668
19. Kuntz ID, Loach PA, Calvin M (1964) Biophys J 4: 227–249
20. Kohl DM, Townsend J, Commoner B, Crespi HL, Dougherty RC, Katz JJ (1965) Nature 206: 1105–1110
21. McElroy JD, Feher G, Mauzerall DC (1972) Biochim Biophys Acta 267: 363–374
22. Feher G, Hoff AJ, Isaacson RA, Ackerson LC (1975) Ann NY Acad Sci 244: 239–259
23. Druyan ME, Norris JR, Katz JJ (1973) J Am Chem Soc 95: 1682–1683
24. Norris JR, Uphaus RA, Crespi HL, Katz JJ (1971) Proc Natl Acad Sci USA 68: 625–628
25. Kip AP, Kittel C, Levy RA, Portis AM (1953) Phys Rev 91: 1066–1071
26. Feher G, Hoff AJ, McElroy JD, Isaacson RA (1973) Biophys J 13: 61a (abstr. WPM-H7)
27. Norris JR, Druyan ME, Katz JJ (1973) J Am Chem Soc 95: 1680–1682
28. Norris JR, Scheer H, Druyan ME, Katz JJ (1974) Proc Natl Acad Sci USA 71: 4897–4900
29. Norris JR, Scheer H, Katz JJ (1975) Ann NY Acad Sci 244: 260–280
30. Scheer H, Katz JJ, Norris JR (1977) J Am Chem Soc 99: 1372–1381
31. Borg DC, Forman A, Fajer J (1976) J Am Chem Soc 98: 6889–6893
32. Hoff AJ, Möbius K (1978) Proc Natl Acad Sci USA 75: 2296–2300
33. Fajer J, Davis MS, Holten JA, Parson WW, Thornber JP, Windsor MW (1977) 4th Int. Congr. on Photosynth, Reading, UK (abstr. 108)
34. Fajer J, Davis MS, Brune DC, Forman A, Thornber JP (1978) J Am Chem Soc 100: 1918–1920
35. Katz JJ, Norris JR, Shipman LL, Thurnauer MC, Wasielewski MR (1978) Annu Rev Biophys Bioengin 7: 393–434
36. Hoff AJ (1982) In: Fong FK (ed) Light reaction pathway of photosynthesis. Springer, Berlin Heidelberg New York
37. Katz JJ, Norris JR (1973) In: Sanadi DR, Packer L (eds) Current topics bioenergetics, vol 5. Academic Press, New York, pp 41–75
38. Fong FK (1974) Proc Natl Acad Sci USA 71: 3692–3695
39. Wasielewski MR, Svec WA, Cope BT (1978) J Am Chem Soc 100: 1961–1962
40. Shipman LL, Cotton TM, Norris JR, Katz JJ (1976) Proc Natl Acad Sci USA 73: 1791–1794
41. Lutz M, Hoff AJ, Brehamet L (1982) Photochem Photobiol (in press)
42. Hoff AJ (1982) In: Clarke RH (ed) Triplet state ODMR spectroscopy: Techniques and applications to biological systems, chap 9. John Wiley & Sons, New York
43. Lubitz W, Lendzian F, Scheer H, Möbius K (1981) J Am Chem Soc 103: 4635–4637
44. Warden JT, Bolton JR (1974) Photochem Photobiol 20: 251–262
45. Kok B (1961) Biochim Biophys Acta 48: 527–533
46. Ke B, Sugahara K, Shaw ER (1975) Biochim Biophys Acta 408: 12–25
47. Calvin M, Androes GM (1962) Science 138: 867–873
48. Knaff DB, Malkin R (1973) Arch Biochem Biophys 159: 555–562
49. Evans MCW, Sihra CK, Slabas AR (1977) Biochem J 162: 75–85

50. Williams-Smith DL, Heathcote P, Sihra CK, Evans MCW (1978) Biochem J 170: 365–371
51. Setif P, Mathis P (1980) Arch Biochem Biophys 204: 477–485
52. Norris JR, Thurnauer MC, Bowman MK, Trifunac AD (1978) In: Dutton PL et al (eds) Frontiers of biological energetics, vol 1. Academic Press, New York, pp 581–592
53. Warden JT, Bolton JR (1972) J Am Chem Soc 94: 4352–4353
54. Warden JT, Bolton JR (1974) Photochem Photobiol 20: 263–269
55. Warden JT, Mohanty P, Bolton JR (1974) Biochem Biophys Res Commun 59: 872–878
56. Visser JWM, Rijgersberg CP, Amesz J (1974) Biochim Biophys Acta 368: 235–246
57. Ke B, Sugahara K, Sahu S (1976) Biochim Biophys Acta 449: 84–94
58. Ke B, Dolan E, Sugahara K, Hawkridge FM, Demeter S, Shaw ER (1977) In: Photosynthetic organelles. Special Issue: Plant Cell Physiol No 3: 187–199
59. Ke B, Demeter S, Zamaraev KI, Khairutdinov RF (1979) Biochim Biophys Acta 546: 265–284
60. Bukhov NG, Karapetyan NV (1978) Mol Biol (Moscow) 12: 868–877
61. Bearden AJ, Malkin R (1977) Brookhaven Symp Biol 28: 247–266
62. Demeter S, Ke B (1978) Biochim Biophys Acta 462: 770–774
63. Evans EH, Cammack R, Evans MCW (1976) Biochem Biophys Res Commun 68: 1212–1218
64. McIntosh AR, Chu M, Bolton JR (1975) Biochim Biophys Acta 376: 308–314
65. Evans MCW, Cammack R (1975) Biochem Biophys Res Commun 63: 187–193
66. Evans MCW, Sihra CK, Bolton JR, Cammack R (1975) Nature 256: 668–670
67. McIntosh AR, Bolton JR (1976) Biochim Biophys Acta 430: 555–559
68. Wasielewski MR, Norris JR, Shipman LL, Lin CP, Svec WA (1981) Biophys J 33: 20a (abstr. M-AM-E7)
69. Olson JM, Thornber JP (1979) In: Capaldi RA (ed) Membrane proteins in energy transduction Marcel Dekker, New York, pp 279–340
70. Dutton PL, Prince RC, Tiede DM (1978) Photochem Photobiol 28: 939–949
71. Davis MR, Forman A, Fajer J (1979) Proc Natl Acad Sci USA 76: 4170–4174
72. Olson JM, Prince RC, Brune DC (1977) Brookhaven Symp Biol 28: 238–246
73. Swarthoff T, Amesz J (1979) Biochim Biophys Acta 548: 427–432
74. Swarthoff T, van der Veek-Horsley KM, Amesz J (1981) Biochim Biophys Acta 635: 1–12
75. Swarthoff T, Gast P, Hoff AJ (1981) FEBS Lett 127: 83–86
76. Swarthoff T, Gast P, Hoff AJ, Amesz J (1981) FEBS Lett 130: 93–98
77. Jennings JV, Evans MCW (1977) FEBS Lett 75: 33–36
78. Knaff DB, Olson JM, Prince RC (1979) FEBS Lett 98: 285–289
79. McElroy JD, Mauzerall DC, Feher G (1974) Biochim Biophys Acta 333: 261–277
80. Lozier RH, Butler WL (1974) Biochim Biophys Acta 333: 465–480
81. Visser JWM, Rijgersberg CP (1975) In: Avron M (ed) Proc 3rd Int Congr Photosynthesis. Elsevier, Amsterdam, pp 397–402
82. Visser JWM, Rijgersberg CP, Gast P (1977) Biochim Biophys Acta 460: 36–46
83. Malkin R, Bearden AJ (1975) Biochim Biophys Acta 396: 250–259
84. Goldfield MG, Halikov RI, Hangulov SV, Kononenko AA, Knox PP (1978) Biochem Biophys Res Commun 85: 1199–1203
85. Van Gorkom HJ, Pulles MPJ, Wessels JSC (1975) Biochim Biophys Acta 408: 331–339
86. Ke B, Sahu S, Shaw E, Beinert H (1974) Biochim Biophys Acta 347: 36–48
87. Slooten L (1972) Biochim Biophys Acta 275: 208–218
88. Clayton RK, Straley SC (1972) Biophys J 12: 1221–1234
89. McElroy JD, Feher G, Mauzerall D (1970) Biophys J 10: 204a (abstr. F-AM-E7)
90. Feher G (1971) Photochem Photobiol 14: 373–387
91. Loach PA, Hall RL (1972) Proc Natl Acad Sci USA 69: 786–790
92. Feher G, Okamura MY, McElroy JD (1972) Biochim Biophys Acta 267: 222–226
93. Feher G, Isaacson RA, McElroy JD, Ackerson LC, Okamura MY, (1974) Biochim Biophys Acta 368: 135–139
94. Debrunner PG, Schulz CE, Feher G, Okamura MY (1975) Biophys J 15: 226a (abstr TH-PM-L12)

95. Butler WF, Johnston DC, Shore HB, Fredkin DR, Okamura MY, Feher G (1980) Biophys J 32: 967–992
96. Wraight CA (1978) FEBS Lett 93: 283–288
97. Okamura MY, Isaacson RA, Feher G (1978) Biophys J 21: 8a (abstr M-AM-A4)
98. Eisenberger PM, Okamura MY, Feher G (1980) Fed Proc (abstr 1036)
99. Feher G, Okamura MY (1978) In: Clayton RK, Sistrom WR (eds) The photosynthetic bacteria. Plenum Press, New York, pp 349–386
100. Feher G, Okamura MY (1977) Brookhaven Symp Biol 28: 183–194
101. Blankenship RE, Parson WW (1979) Biochim Biophys Acta 545: 429–444
102. Debus RJ, Okamura MY, Feher G (1981) Biophys J 33: 19a (abstr M-AM-E4)
103. Hales BJ (1975) J Am Chem Soc 97: 5993–5997
104. Hales BJ, Das Gupta A (1979) Biochim Biophys Acta 548: 276–286
105. Vermeglio A (1977) Biochim Biophys Acta 459: 516–524
106. Wraight CA (1977) Biochim Biophys Acta 459: 525–531
107. Gast P, Hoff AJ (1979) Biochim Biophys Acta 548: 520–535
108. Rafferty CN, Clayton RK (1979) Biochim Biophys Acta 546: 189–206
109. Takamiya K, Dutton PL (1977) FEBS Lett 80: 279–284
110. Okamura MY, Debus RJ, Isaacson RA, Feher G (1980) Fed Proc (abstr 1037)
111. Das MR, Connor HD, Leniart DS, Freed JH (1970) J Am Chem Soc 92: 2258–2268
112. Rutherford AW, Heathcote P, Evans MCW (1979) Biochem J 182: 515–523
113. Knaff DB, Malkin R (1976) Biochim Biophys Acta 430: 244–252
114. Evans MCW (1977) In: Barber J (ed) The primary processes of photosynthesis. chap 10. Elsevier/North-Holland Biomedical Press, Amsterdam, pp 434–464
115. Ke B (1973) Biochim Biophys Acta 301: 1–33
116. Malkin R, Bearden AJ (1978) Biochim Biophys Acta 505: 147–181
117. Evans MCW, Reeves SG, Cammack R (1974) FEBS Lett 49: 111–114
118. Heathcote P, Williams-Smith DL, Sihra CK, Evans MCW (1978) Biochim Biophys Acta 503: 333–342
119. Cammack R, Ryan MD, Stewart AC (1979) FEBS Lett 107: 442–446
120. Hootkins R, Malkin R, Bearden A (1981) FEBS Lett 123: 229–234
121. Evans MCW, Sihra CK, Cammack R (1976) Biochem J 158, 71–77
122. Dismukes GC, Sauer K (1978) Biochim Biophys Acta 504: 431–445
123. Dutton PL, Leigh JS (1973) Biochim Biophys Acta 314: 178–190
124. Ke B (1972) Arch Biochem Biophys 152: 70–77
125. Ke B, Beinert H (1973) Biochim Biophys Acta 305: 689–693
126. Golbeck JH, Velthuys BR, Kok B (1978) Biochim Biophys Acta 504: 226–230
127. Mathis P, Conjeaud H (1979) Photochem Photobiol 29: 833–837
128. Cammack R, Evans MCW (1975) Biochem Biophys Res Commun 67: 544–549
129. Heathcote P, Williams-Smith DL, Evans MCW (1978) Biochem J 170: 373–378
130. Prince RC, Thornber JP (1977) FEBS Lett 81: 233–237
131. Prince RC, Crowder MS, Bearden AJ (1980) Biochim Biophys Acta 592: 323–337
132. Blum H, Harmon HJ, Leigh JS, Salerno JC, Chance B (1978) Biochim Biophys Acta 502: 1–10
133. Blum H, Salerno JC, Leigh JS (1978) J Magn Reson 30: 385–391
134. Malkin R, Barber J (1979) Arch Biochem Biophys 193: 169–178
135. Knaff DB (1975) FEBS Lett 60: 331–335
136. Stiehl HH, Witt HT (1969) Z Naturforsch 24b: 1588–1598
137. Van Gorkom HJ (1974) Biochim Biophys Acta 347: 439–442
138. Nugent JHA, Diner BA, Evans MCW (1981) FEBS Lett 124: 241–244
139. Klimov VV, Allakhverdiev SI, Krasnovsky AA (1979) Dokl Akad Nauk 249: 485–488
140. Klimov VV, Dolan E, Shaw ER, Ke B (1980) Proc Natl Acad Sci USA 77: 7227–7231
141. Bouges-Bocquet B (1973) Biochim Biophys Acta 314: 250–256
142. Velthuys BR, Amesz J (1974) Biochim Biophys Acta 333: 85–94
143. Parson WW, Clayton RK, Cogdell RJ (1975) Biochim Biophys Acta 387: 265–278
144. Fajer J, Brune DC, Davis MS, Forman A, Spaulding LD (1975) Proc Natl Acad Sci USA 72: 4956–4960

145. Rockley MG, Windsor MW, Cogdell RJ, Parson WW (1975) Proc Natl Acad Sci USA 72: 2251–2255
146. Kaufmann KJ, Dutton PL, Netzel TL, Leigh LS, Rentzepis PM (1975) Science 188: 1301–1304
147. Rademaker H, Hoff AJ (1981) Biophys J 34: 325–344
148. Wraight CA, Leigh JS, Dutton PL, Clayton RK (1974) Biochim Biophys Acta 333: 401–408
149. Rutherford AW, Evans MCW (1980) FEBS Lett 110: 257–261
150. Shuvalov VA, Klimov VV (1976) Biochim Biophys Acta 440: 587–599
151. Tiede DM, Prince RC, Reed GH, Dutton PL (1976) FEBS Lett 65: 301–304
152. Okamura MY, Isaacson RA, Feher G (1979) Biochim Biophys Acta 547: 394–417
153. Prince RC, Leigh JS, Dutton PL (1976) Biochim Biophys Acta 440: 622–636
154. Prince RC, Tiede DM, Thornber JP, Dutton PL (1977) Biochim Biophys Acta 462: 467–490
155. Klimov VV, Shuvalov VA, Krakhmaleva IN, Klevanik AV, Krasnovskii AA (1977) Biokhimija 42: 519–530
156. Fajer J, Davis MS, Brune DC, Spaulding LD, Borg DC, Forman A (1977) Brookhaven Symp Biol 28: 74–104
157. Davis MS, Forman A, Hanson LK, Thornber JP, Fajer J (1979) J Phys Chem 83: 3325–3332
158. Prince RC (1978) Biochim Biophys Acta 501: 195–207
159. Tiede DM, Prince RC, Dutton PL (1976) Biochim Biophys Acta 449: 447–467
160. Feher G, Isaacson RA, Okamura MY (1977) Biophys J 17: 149a (abstr TH-AM-F12)
161. Van Grondelle R, Romijn JC, Holmes NG (1976) FEBS Lett 72: 187–192
162. Schepler KL, Dunham WR, Sands RH, Fee JH, Abeles RH (1975) Biochim Biophys Acta 399: 510–518
163. Sauer K, Mathis P, Acker S, Van Best JA (1978) Biochim Biophys Acta 503: 120–134
164. Mathis P, Sauer K, Remy R (1978) FEBS Lett 88: 275–278
165. Baltimore BG, Malkin R (1980) FEBS Lett 110: 50–52
166. Thornber JP, Alberte RS, Hunter FA, Shiozawa JA, Kan K-S (1977) Brookhaven Symp Biol 28: 132–148
167. Uphaus RA, Norris JR, Katz JJ (1974) Biochem Biophys Res Commun 61: 1057–1063
168. Fujita I, Davis MS, Fajer J (1978) J Am Chem Soc 100: 6280–6282
169. Shuvalov VA, Dolan E, Ke B (1979) Proc Natl Acad Sci USA 76: 770–773
170. Shuvalov VA, Ke B, Dolan E (1979) FEBS Lett 100: 5–8
171. Baltimore BG, Malkin R (1980) Photochem Photobiol 31: 485–490
172. Heathcote P, Evans MCW (1980) FEBS Lett 111: 381–385
173. Fajer J, Davis MS, Forman A, Klimov VV, Dolan E, Ke B (1980) J Am Chem Soc 102: 7143–7145
174. Hoff AJ, Lendzian F, Lubitz W, Möbius K (1982) Chem Phys Lett 85: 3–8
175. Klimov VV, Klevanik AV, Shuvalov VA, Krasnovskii AA (1977) FEBS Lett 82: 183–186
176. Rademaker H, Hoff AJ, Duysens LNM (1979) Biochim Biophys Acta 546: 248–255
177. Klimov VV, Allakhverdiev SI, Demeter S, Krasnovsky AA (1979) Dokl Akad Nauk 249: 227–230
178. Rutherford AW, Mullet JE, Crofts AR (1981) FEBS Lett 123: 235–237
179. Klimov VV, Dolan E, Ke B (1980) FEBS Lett 112: 97–100
180. Blankenship RE, Parson WW (1978) Annu Rev Biochem 47: 635–653
181. Blankenship RE, Parson WW (1979) In: Barber J (ed) Photosynthesis in relation to model systems, chap 3. Elsevier/North-Holland Biomedical Press, Amsterdam, pp 71–114
182. Godik VI, Borisov AY (1979) Biochim Biophys Acta 548: 296–308
183. Godik VI, Borisov AY (1980) Biochim Biophys Acta 593: 182–193
184. Van Bochove AC, van Grondelle R, Duysens LNM (1981) In: Akoyunoglu G (ed) Proc 6th Int. Congress on Photosynthesis, Halkidiki, Greece, 1980
185. Parson WW, Monger TG (1977) Brookhaven Symp Biol 28: 195–212
186. Dutton PL, Leigh JS, Seibert M (1971) Biochem Biophys Res Commun 46: 406–413
187. Leigh JS, Dutton PL (1974) Biochim Biophys Acta 357: 67–77

188. Schaafsma TJ, Kleibeuker JF, Platenkamp RJ, Geerse P (1976) In: Proc 12th Eur. Congr. Molec. Spectroscopy, Strasbourg, France, pp 491–494
189. Thurnauer MC, Katz JJ, Norris JR (1975) Proc Natl Acad Sci USA 72: 3270–3274
190. Hoff AJ (1981) Q Rev Biophys 14: 599–665
191. Norris JR, Uphaus RA, Katz JJ (1975) Chem Phys Lett 31: 157–161
192. Thurnauer MC, Norris JR (1977) Chem Phys Lett 47: 100–105
193. Clarke RH, Connors RE, Frank HA, Hoch JC (1977) Chem Phys Lett 45: 523–528
194. Levanon H, Norris JR (1978) Chem Rev 78: 185–198
195. Gast P, Hoff AJ (1978) FEBS Lett 85: 183–188
196. Mushlin RA, Gast P, Hoff AJ (1980) Chem Phys Lett 76: 542–547
197. Hoff AJ (1976) Biochim Biophys Acta 440: 765–771
198. Hoff AJ, Gorter de Vries H (1978) Biochim Biophys Acta 503: 94–106
199. Clarke RH, Connors RE, Norris JR, Thurnauer MC (1975) J Am Chem Soc 97: 7178–7179
200. Clarke RH, Connors RE, Frank HA (1976) Biochem Biophys Res Commun 71: 671–675
201. Hoff AJ, Cornelissen B (1982) Mol Phys (in press)
202. Hägele WU (1977) Thesis, University of Stuttgart
203. Clarke RH (ed) (1981) Triplet state ODMR spectroscopy: Techniques and applications to biological systems. John Wiley & Sons, New York
204. Kooyman RPH, Schaafsma TJ (1980) J Mol Struct 60: 373–380
205. Schweitzer D, Hausser KH, Taglieber V, Staab HA (1976) Chem Phys 14: 183–189
206. Goldacker W, Hausser KH, Schweitzer D, Staab HA (1979) J Lumin 18/19: 415–419
207. Thurnauer MC, Norris JR (1976) Biochem Biophys Res Commun 73: 501–506
208. Thurnauer MC, Norris JR (1977) Chem Phys Lett 47: 100–105
209. Boxer SG, Roelofs MG (1979) Proc Natl Acad Sci USA 76: 5636–5640
210. Frank HA, Bolt J, Friesner R, Sauer K (1979) Biochim Biophys Acta 547: 502–511
211. Frank HA, Friesner R, Nairn JA, Dismukes GC, Sauer K (1979) Biochim Biophys Acta 547: 484–501
212. Vermeglio A, Breton J, Paillotin G, Cogdell R (1978) Biochim Biophys Acta 501: 514–530
213. Frank HA, McLean MB, Sauer K (1979) Proc Natl Acad Sci USA 76: 5124–5128
214. Rutherford AW, Paterson DR, Mullet JE (1981) In: Akoyunoglu G (ed) Proc. 5th Int. Congr. on Photosynthesis. Halkidiki, Greece, 1980
215. Holten D, Windsor M, Parson WW, Gouterman M (1978) Photochem Photobiol 28: 951–961
216. Blankenship RE, McGuire A, Sauer K (1975) Proc Natl Acad Sci USA 72: 4943–4947
217. McIntosh AR, Bolton JR (1976) Nature 263: 443–445
218. Dismukes GC, McGuire A, Blankenship R, Sauer K (1978) Biophys J 21: 239–256
219. Friesner R, Dismukes GC, Sauer K (1979) Biophys J 25: 277–294
220. McIntosh AR, Manikowski H, Bolton JR (1979) J Phys Chem 83: 3309–3313
221. McIntosh AR, Manikowski H, Wong SK, Taylor CPS, Bolton JR (1979) Biochem Biophys Res Commun 87: 605–612
222. McIntosh AR, Manikowski H, Bolton JR (1981) In: Akoyunoglu G (ed) Proc. 5th Int. Congr. on Photosynthesis, Halkidiki, Greece, 1980
223. Sauer K, Frank HA, McCracken JL (1981) In: Akoyunoglu G (ed) Proc. 5th Int. Congr. on Photosynthesis, Halkidiki, Greece, 1980
224. Warden JT, Adrianowycz OL (1981) In: Akoyunoglu G (ed) Proc. 5th Int. Congr. on Photosynthesis, Halkidiki, Greece, 1980
225. Hoff AJ, Gast P, Romijn JC (1977) FEBS Lett 73: 185–190
226. Hoff AJ, Gast P (1979) J Phys Chem 83: 3355–3358
227. Blankenship RE (1981) Acc Chem Res 14: 163–170
228. Pedersen JB (1979) FEBS Lett 97: 305–310
229. Gast P, Mushlin RA, Hoff AJ (1982) J Phys Chem (in press)
230. Haberkorn R, Michel-Beyerle ME, Marcus RA (1979) Proc Natl Acad Sci USA 76: 4185–4188
231. Shuvalov VA, Parson WW (1981) Proc Natl Acad Sci USA 78: 957–961

232. Shuvalov VA, Parson WW (1981) In: Akoyunoglu G (ed) Proc. 5th Int. Congr. on Photosynthesis, Halkidiki, Greece, 1980
233. Kaplan DE, Browne ME, Lowen JA (1961) Rev Sci Instrum 32: 1182–1186
234. Mims WB, Nassau K, McGee JD (1961) Phys Rev 123: 2059–2069
235. Thurnauer MC, Bowman MK, Norris JR (1979) FEBS Lett 100: 309–312
236. Thurnauer MC, Norris JR (1980) Chem Phys Lett 76: 557–561
237. Nishi N, Hoff AJ, Van der Waals JH (1980) Biochim Biophys Acta 590: 74–88
238. Nishi N, Hoff AJ, Schmidt J, Van der Waals JH (1978) Chem Phys Lett 58: 164–170
239. Gast P, Mushlin RA, Hoff AJ (1981) In: Akoyunoglu, G. (ed) Proc. 5th Int. Congr. on Photosynthesis, Halkidiki, Greece, 1980
240. Bowman MK, Norris JR (1981) J Am Chem Soc (in press)
241. Hoff AJ, Gast P, Isaacson RA, Feher G (1981) In: Akoyunoglu G (ed) Proc. 5th Int. Congr. on Photosynthesis, Halkidiki, Greece, 1980
242. Borg DC, Fajer J, Felton RH, Dolphin D (1970) Proc Natl Acad Sci USA 67: 813–820
243. Fajer J, Borg DC, Forman A, Felton RH, Dolphin D, Vegh L (1974) Proc Natl Acad Sci USA 71: 994–998
244. Fajer J, Forman A, Davis MS, Spaulding LD, Brune DC, Felton RH (1977) J Am Chem Soc 99: 4134–4140
245. Kleibeuker JF, Schaafsma TJ (1974) Chem Phys Lett 29: 116–122
246. Swarthoff T, Gast P, van der Veek-Horsley KM, Hoff AJ, Amesz J (1981) FEBS Lett 131: 331–334
247. Forman A, Davis MS, Fujita I, Hanson LK, Smith KM, Fajer J (1981) Isr J Chem (in press)
248. Rutherford AW, Mullet JE (1981) Biochim Biophys Acta 635: 225–235
249. Rutherford AW, Paterson DR, Mullet JE (1981) Biochim Biophys Acta 635: 205–214
250. Hales BJ, Case EE (1981) Biochim Biophys Acta 637: 291–302
251. Hiyama T, Fork DC (1980) Arch Biochem Biophys 199: 488–496
252. Asa R, Bergström J, Vånngård T (1981) Biochim Biophys Acta 637: 118–123
253. Setif P, Hervo G, Mathis P (1981) Biochim Biophys Acta 638: 257–267
254. Bowman MK, Budil DE, Closs GL, Kosta AG, Wraight CA, Norris JR (1981) Proc Natl Acad Sci USA 78: 3305–3307

Received May 29, 1981/Accepted October 2, 1981

Notes added in proof

Section 4.1.1. The variation in g-value and linewidth of the ESR signal of uncomplexed uQ_1^- in vivo has been explained by Hales and Case [250] on the basis of a study of semiquinones in vitro as a result of differences in proticity of the environment of uQ_1^-.

Section 4.2. A study by Hiyama and Fork [251] of the kinetics of the 430 nm absorption change at 20° and 0° C and of the dark recovery of $F_{X,B,A}$ by low temperature ESR after quick-freezing, suggests that F_X rather than $F_{B,A}$ is responsible for the 430 nm absorption upon reduction.

Aasa et al.[252] have performed Q-band (35 Hz) ESR spectroscopy on $F_B^-F_A^-$. In agreement with the 24 GHz results ([1] and Fig. 7b) they find a spectrum that is very similar on a g-scale to the X-band spectrum of $F_B^-F_A^-$. As in [1], the conclusion is that F_B^- and F_A^- interact weakly (interaction energy of the order of 0.01 cm^{-1}). This relatively weak interaction, however, may be sufficient to generate the various changes of the F_B^- or the F_A^- spectrum in the singly reduced F_BF_A complex compared to the doubly reduced $F_B^-F_A^-$ complex.

Section 5.2. Recently, Setif et al. [253] have measured flash-induced optical difference spectra of PS 1 particles (CP 1) at 21° C and 10 K. They conclude that, as suggested in [1] and [36], the 1 ms component arises from the decay of the triplet state of P700.

Section 7. Bowman et al. [254] have performed pulsed ESR of the transient state $P860^{+}Bph^{-}(uQ_1^{-})$ of reaction centers of *Rps. sphaeroides* R-26 employing optical detection via the absorption at 860 nm. Microwaves resonant between two of the four radical pair energy levels influence the singlet-triplet mixing, and consequently the steady-state concentration of P860. High microwave powers (in excess of 1 kW) are required to have insufficient transition probability during the short lifetime of the radical pair. With uQ_1^{-} present the linewidth of the signal due to the transient biradical was 210 G; in uQ_1-free reaction centers the width was 64 G. These results are discussed in terms of exchange and dipole-dipole interactions between the geminate radicals.